AD_____

Award Number: W81XWH-12-1-0234

TITLE: The Role of a Novel Myosin Isoform in Prostate Cancer Metastasis

PRINCIPAL INVESTIGATOR: Wilma A. Hofmann, Ph.D.

CONTRACTING ORGANIZATION: State University of New York, Buffalo, Buffalo, NY 14260-0001

REPORT DATE: October 2013

TYPE OF REPORT: Annual

PREPARED FOR: U.S. Army Medical Research and Materiel Command
Fort Detrick, Maryland 21702-5012

REPORT DOCUMENTATION PAGE

Form Approved
OMB No. 0704-0188

1. REPORT DATE	2. REPORT TYPE	3. DATES COVERED
October 2013	Annual	30 September 2012-29 September 2013

4. TITLE AND SUBTITLE
The Role of a Novel Myosin Isoform in Prostate Cancer Metastasis

5a. CONTRACT NUMBER

5b. GRANT NUMBER
W81XWH-12-1-0234

5c. PROGRAM ELEMENT NUMBER

6. AUTHOR(S)
Wilma A. Hofmann

E-Mail: whofmann@buffalo.edu

5d. PROJECT NUMBER

5e. TASK NUMBER

5f. WORK UNIT NUMBER

7. PERFORMING ORGANIZATION NAME(S) AND ADDRESS(ES)

State University of New York, Buffalo, Buffalo, NY 14260-0001

8. PERFORMING ORGANIZATION REPORT NUMBER

9. SPONSORING / MONITORING AGENCY NAME(S) AND ADDRESS(ES)
U.S. Army Medical Research and Materiel Command
Fort Detrick, Maryland 21702-5012

10. SPONSOR/MONITOR'S ACRONYM(S)

11. SPONSOR/MONITOR'S REPORT NUMBER(S)

12. DISTRIBUTION / AVAILABILITY STATEMENT
Approved for Public Release; Distribution Unlimited

13. SUPPLEMENTARY NOTES

14. ABSTRACT

The objective of the project for the reporting period was to generate a number prostate cancer cell lines that that are either myosin IC isoform A deficient or that constitutively express GFP-myosin IC isoform A. We used shRNA to generate isoform A-negative PC-3 cells and we generated a stable LNCaP cell line that expresses constitutively myosin IC isoform A-GFP. We are now in the process of analyzing the effect of these expression changes on secretion in these cell lines to determine the consequences of isoform A expression changes for the metastatic ability of prostate cancer cells. Using serial cloning of the 5 prime UTR of the human myosin IC gene we have identified a region that is involved in regulatory expression of myosin IC isoform A. We are now in the process of using ChIP assays to identifying the transcriptional elements that bind to this region and induce expression of myosin IC isoform A in prostate cancer cells.

15. SUBJECT TERMS
Myosin IC, isoform A, prostate cancer, shRNA, invasion, ChIP assay, promoter

16. SECURITY CLASSIFICATION OF:			17. LIMITATION OF ABSTRACT	18. NUMBER OF PAGES	19a. NAME OF RESPONSIBLE PERSON
a. REPORT	b. ABSTRACT	c. THIS PAGE			USAMRMC
U	U	U	UU	31	19b. TELEPHONE NUMBER *(include area code)*

Table of Contents

	Page
Introduction……..	**4**
Body……..	**4-6**
Key Research Accomplishments……..	**6**
Reportable Outcomes……	**7**
Conclusion……	**7**
References……	**7**
Appendices……	**8-31**

INTRODUCTION

We recently discovered a previously unknown isoform of myosin IC that is called myosin IC isoform A [1]. Our data showed that this isoform is selectively expressed in prostate cancer tumors and in prostate cancer cell lines with high metastatic potential but not in normal prostate tissues or in prostate cancer cells with low metastatic potential. Class I myosins are involved in intracellular transport of vesicles that are secreted [2] and our preliminary data suggest that overexpression of myosin IC isoform A in prostate cancer cells causes an increase in secretion efficiency. Secretion is a process that is intricately linked to the acquisition of a metastatic phenotype in cancer cells. In order to move away from the site of a primary tumor and invade other tissues, cancer cells must degrade and remodel the extracellular material that surrounds them which is a achieved through secretion of specific proteins and factors into the extracellular environment [3-5]. We postulate that the increase in secretion efficiency due to overexpression of myosin IC isoform A is causally linked to an increased metastatic potential of prostate cancer cells. We have planned a series of experiments to **(i)** determine how this myosin isoform contributes to the invasive phenotype of cancer cells, **(ii)** identify the transcriptional elements that regulate selective expression of this isoform and **(iii)** explore the potential of this isoform as a diagnostic marker for progressive prostate cancer.

BODY

Tasks outlined in the approved Statement of Work for this period of the project

Task 1.a. **Generate isoform A negative and positive cell lines (Months 1-12).**
Task 1.b. **Test the effect of isoform A expression on secretion and secreted components (Months 6-24).**

Task 2.a. **Identify regulatory elements in the 5' gene region of isoform A (Months 6-24).**

Task 3.a. **Analyze isoform A mRNA and protein expression in murine prostate cancer (Months 9-24).**
Task 3.b. **Perform histopathological analysis of metastatic and normal tissue from mouse (Month 9-36).**
Task 3.c. **Analyze murine blood/serum samples for detection of isoform A. (Month 9-24)**

Our progress/accomplishments associated with the tasks are as follows:

1. Generation of isoform A positive LNCaP cell lines. Our preliminary data showed that myosin IC isoform A is expressed in the highly invasive prostate cancer cell line PC-3 but not in the low invasive prostate cancer cell line LNCaP on both, protein level (Fig. 1A) and on mRNA level (Fig. 1B) while other myosin IC isoforms are expressed at comparable levels in both cell types (shown in Figure 1 is a comparison of myosin IC

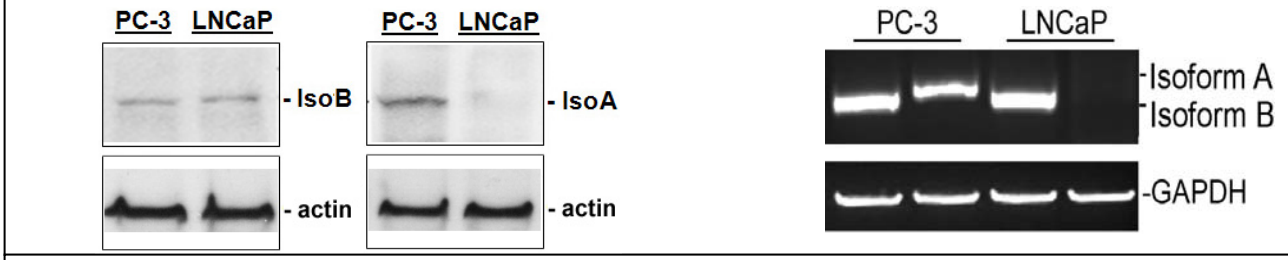

Figure 1: Selective expression of myosin IC isoforms in prostate cancer cell lines. *A: Representative depiction of isoform A and B protein expression in PC-3 and LNCaP cells.* Immunoblot analysis of PC-3 and LNCaP cell extracts. Proteins were separated by SDS PAGE and transferred to nitrocellulose. The membrane was cut at appropriate sites and the samples were analyzed with isoform specific antibodies and with antibodies to actin as loading control. Isoform B is present in both cell lines at comparable levels while isoform A protein is only expressed in PC-3 cells. *B: Representative depiction of isoform A and B mRNA expression in PC-3 and LNCaP cells.* End-point PCR with isoform B (lanes 1&3) and A (lanes 2&4) specific primer showed that isoform B is expressed in both cell types at comparable levels while isoform A is only expressed in PC-3. GAPDH was co-amplified as control.

isoform B and isoform A). To determine the effect of isoform expression on the metastatic ability of cells, we proposed to generate a LNCaP cell line (naturally isoform A negative) that constitutively expresses isoform A so that isoform A negative and isoform A positive LNCaP cells can be compared in later assays. To generate the LNCaP positive cell line, we cloned the sequence coding for mouse myosin IC isoform A into a mammalian GFP expression vector that also encodes a kanamycin resistance for selection in bacteria and a neomycin (G418) resistance for selection in mammalian cells. Cells were then transfected with this construct and selection of stably expressing cells was performed by treating the cells with G418 that kills cells that do not have the GFP plasmid. As shown in Fig. 2, we have been successful in generating a LNCaP cell line (LNCaP-isoform A) that stably expresses myosin IC isoform A-GFP.

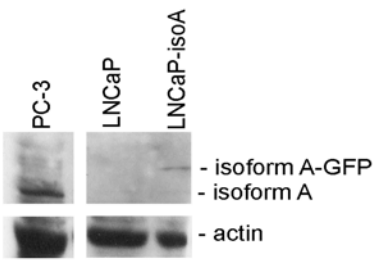

Figure 2: Generation of LNCaP-isoA, a cell line that stably expressed myosin IC isoform A-GFP. Immunoblot analysis of cell extract from PC-3, LNCaP, and LNCaP –isoA which stably express myosin IC isoform A-GFP. Proteins were separated by SDS PAGE and transferred to nitrocellulose. The membrane was cut at appropriate sites and the samples were analyzed with antibodies specific to isoform A and with antibodies to actin as loading control. Note that PC-3 cells (left lane) express isoform A while LNCaP cells are isoform A negative (middle lane). However LNCaP-isoA cells stably express isoform A-GFP (right lane).

2. Generation of isoform A negative PC-3 cell lines. In contrast to LNCaP cells, PC-3 cells express endogenous isoform A. We planned to generate a isoform A-negative PC-3 cells by generating a cell line that stably expresses isoform A-shRNA which would cause a constitutive repression of myosin IC isoform A. However, during the process of generating this isoform A negative cell line we noticed that PC-3 cells at a specific passage stop expression of isoform A by themself. We don't know the passage number of the PC-3 cells therefore we count passage from the time the cell came to our lab starting with passage 1. As shown in Figure 3, PC-3 cells stop expression of isoform A between passage p20-p25. This has a number of implications. First of all, one could argue that we were anyway in the process of generating a isoform A negative PC-3 cell line and therefore we could as well use these cells that have stopped expressing isoform A. However, we are disinclined to do so because at this point we cannot be sure what other genes at this time have altered expression profiles and thus our data could not be related directly to changes specifically in isoform A expression. Secondly, because cells stop expressing isoform A at a relative early passage (between p20-p25) we can not proceed with the original plan of generating a stably expressing isoform A-shRNA cell line because it takes too many passages to generate this, i.e. by the time we have generated a stably isoform A-repressed cell line, the culture cells will have altered their expression profile. Therefore, we will now turn to plan B and instead of working with stale isoform A-negative cell lines, we will use transient transfections of shRNAs.

Confirming the unexplained and unexpected stop of isoform A expression in PC-3 cells at a certain passage and the discovery that creating stable shRNA expressing cell lines is not a viable approach because only very few passages are left after cells stably express the shRNA and before losing endogenous expression, took the most part of year 1. We are currently in the process of optimizing the method of transient siRNA expression such as optimization of transfection efficiency, control of knock down efficiency etc.

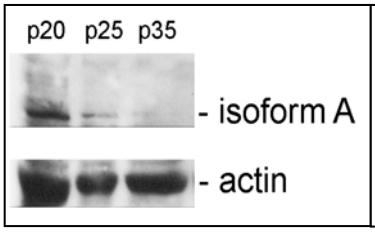

Figure 3: PC-3 cells stop expression of isoform A at a defined passage. Immunoblot analysis of cell extract from PC-3 cells from the indicate passage Proteins were separated by SDS PAGE and transferred to nitrocellulose. The membrane was cut at appropriate sites and the samples were analyzed with antibodies specific to isoform A and with antibodies to actin as loading control. Note that PC-3 cells stop expression of isoform A between passage p20-p25.

3. Test the effect of isoform A expression on secretion and secreted components

This task relies on the tools generated in task 1a. Due to the unexpected delay in generating a PC-3 negative cell line caused by loss of endogenous isoform A expression at a certain passage (Fig. 1B), we have not yet been able to proceed to Task 1.b.. However, our data indicate that using the siRNA approach will be

effective. As soon as we have performed the appropriate controls, we will proceed to the studies proposed for task 1.b. and test the created isoform A-positive LNCaP and isoform A-negative PC-3 cells in the invasion and migration assays as planned.

4. Identification of two regulatory elements in the 5' upstream genomic region of isoform A.

Our preliminary data suggested that a synergistic action of at least two regulatory sites is involved in transcription activation of isoform A in PC-3 cells. To identify these elements, we used the Luciferase Reporter Assay System. Specifically, we cloned the 5' region of myosin IC isoform A into a luciferase vector. We then performed serial deletion of this region and measured the effect of specific deletions on expression of luciferase in PC-3 cells to identify the regulatory regions of the myosin IC gene that are involved in expression of isoform A. As shown in Figure 4, we identified two ~50bp long regions in the 5' region. The first region is located between base pairs 700 and 647 and the second between base pairs 482 and 438 upstream of the translation start site. We are currently in the process of screening these sites for potential transcription factor binding sites using various transcription factor binding site prediction programs including MATCH [6], TESS (transcription element search system) and TRANSFAC [7].

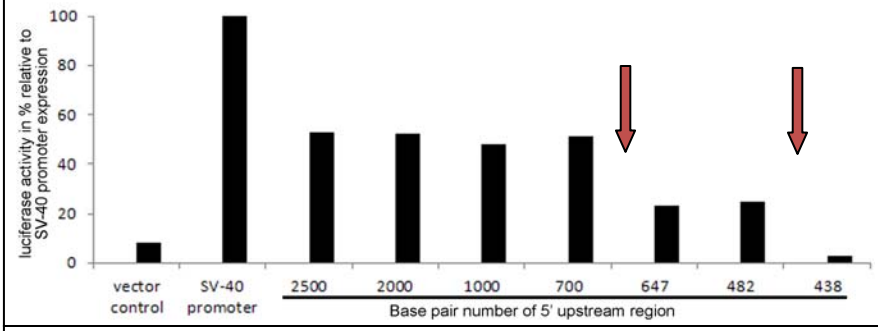

Figure 4: Two regulatory elements are present in the 2500bp long 5' upstream region of isoform A. Luciferase assays were performed in PC-3 cells with fragments of the indicated length and relative luciferase activity was measured as described. 2 significant drops in luciferase activity were observed (indicated by arrows. A first drop occurred after reducing the fragment from 700bp to 647bp, indicating the location of a regulatory site. A second final drop was observed after deleting a 40bp long fragment located ~450bp upstream of isoform A. These data suggest that a second regulatory element is located within these 40bp.

5. Analysis of murine tissue and serum samples for expression of myosin IC isoform A.

Tasks 3.a-c. are to analyze murine normal and tumor tissue samples and blood/serum samples from the TRAMP prostate cancer mouse model [8] for expression of isoform A. Because of the unexpected difficulties in creating a PC-3 cell line that is negative for isoform A expression as described above for Task 1.a.(Fig. 3), we are behind in our timeline for the proposed experiments. We have already obtained tissue samples and histological slides for the analysis but we have not yet been able to actually start these experiments. However, based on the progress in creating isoform A-negative PC-3 cells using the alternative approach of transient transfection as described above under point 2, we are confident that we will have completed this task 1.a. in the next two month and we will then move on to tasks 3a-c.

KEY RESEARCH ACCOMPLISHEMENTS

(i) We have generated the cell line LNCaP-isoform A that stably expresses myosin IC isoform A-GFP.
(ii) Using shRNA and siRNA transfections, we are in the process of optimizing the best method to repress isoform A expression in PC-3 cells.
(iii) By using serial deletion of myosn IC isoform sequences followed by immunofluorescence analysis of the various myosin IC isoform constructs, we confirmed that the newly identified myosin IC isoform A shows a isoform specific cellular localization and functions related to cytoplasmic secretion.
(iv) By using serial deletion experiments of the 5' region of the myosin IC gene coupled with luciferase assays, we identified two regulatory domains in the 5'region that are involved in selective expression of myosin IC isoform A.

REPORTABLE OUTCOMES: The research performed directly or indirectly contributed to the following publications and poster abstracts.

Publications:

1. Schwab, R.S., Ihantovych, I., Yunus, S.Z.S.A., Domaradzki, T. and **Hofmann, W.A.** (2013). Identification of Signals that Facilitate Isoform Specific Nucleolar Localization of Myosin IC. *Exp. Cell Res.* 319 (8): 1111-1123.
2. Simon, D.N., Domaradzki, T., **Hofmann, W.A.** and Wilson, K. L. (2013). Lamin A tail modification by SUMO1 is disrupted by familial partial lipodystrophy-causing mutations. *Mol. Biol. Cell*, 24(3): 342-50.

Meeting abstracts:

1. Domaradzki, T. and Hofmann, W.A.: The role of myosin IC isoform A in prostate cancer metastasis. **Poster presentation at the 9th *Annual Celebration of Academic Excellence,* Buffalo, NY, April 2013.**
2. Schwab, R. and Hofmann, W.A.: Identification and characterization of posttranslational modifications of myosin IC. **Poster presentation at the 9th *Annual Celebration of Academic Excellence,* Buffalo, NY, April 2013.**

CONCLUSION: With creating the LNCaP cell line that stably expresses myosin IC isoform A and by identifying the best way to prevent expression of myosin IC isoform A in PC-3 cells we have generated the tools that were needed to proceed to the analysis of the effect of myosin IC isoform A expression on the acquisition of a metastatic phenotype in prostate cancer cells.
We further identified the genomic region that is involved in selective expression of myosin IC isoform A and are now in the process of identifying the regulatory elements and transcription factors that are involved in this selective expression.

REFERENCES

[1] I. Ihnatovych, M. Migocka-Patrzalek, M. Dukh, W.A. Hofmann, Identification and characterization of a novel myosin Ic isoform that localizes to the nucleus, Cytoskeleton (Hoboken) 69 (2012) 555-565.

[2] J.L. Welton, S. Khanna, P.J. Giles, P. Brennan, I.A. Brewis, J. Staffurth, M.D. Mason, A. Clayton, Proteomics analysis of bladder cancer exosomes, Mol Cell Proteomics 9 (2010) 1324-1338.

[3] L.A. Liotta, K. Tryggvason, S. Garbisa, I. Hart, C.M. Foltz, S. Shafie, Metastatic potential correlates with enzymatic degradation of basement membrane collagen, Nature 284 (1980) 67-68.

[4] A.R. Nelson, B. Fingleton, M.L. Rothenberg, L.M. Matrisian, Matrix metalloproteinases: biologic activity and clinical implications, J Clin Oncol 18 (2000) 1135-1149.

[5] D. Sliva, Signaling pathways responsible for cancer cell invasion as targets for cancer therapy, Curr Cancer Drug Targets 4 (2004) 327-336.

[6] A.E. Kel, E. Gossling, I. Reuter, E. Cheremushkin, O.V. Kel-Margoulis, E. Wingender, MATCH: A tool for searching transcription factor binding sites in DNA sequences, Nucleic Acids Res 31 (2003) 3576-3579.

[7] V. Matys, O.V. Kel-Margoulis, E. Fricke, I. Liebich, S. Land, A. Barre-Dirrie, I. Reuter, D. Chekmenev, M. Krull, K. Hornischer, N. Voss, P. Stegmaier, B. Lewicki-Potapov, H. Saxel, A.E. Kel, E. Wingender, TRANSFAC and its module TRANSCompel: transcriptional gene regulation in eukaryotes, Nucleic Acids Res 34 (2006) D108-110.

[8] A.A. Hurwitz, B.A. Foster, J.P. Allison, N.M. Greenberg, E.D. Kwon, The TRAMP mouse as a model for prostate cancer, Curr Protoc Immunol Chapter 20 (2001) Unit 20 25.

APPENDICES: Two reprints and two poster abstracts are attached.

EXPERIMENTAL CELL RESEARCH 319 (2013) 1111–1123

Available online at www.sciencedirect.com

SciVerse ScienceDirect

journal homepage: www.elsevier.com/locate/yexcr

Identification of signals that facilitate isoform specific nucleolar localization of myosin IC

Ryan S. Schwab[1], *Ivanna Ihnatovych*[1], *Sharifah Z.S.A. Yunus, Tera Domaradzki, Wilma A. Hofmann**

Department of Physiology and Biophysics, University at Buffalo—State University of New York, Buffalo, NY, USA

ARTICLE INFORMATION

Article Chronology:
Received 3 November 2012
Received in revised form
13 February 2013
Accepted 14 February 2013
Available online 21 February 2013

Keywords:
Myosin IC
Isoforms
Nucleolar localization signal
Nucleolus
Nucleus
RNA polymerase I
Fibrillarin

ABSTRACT

Myosin IC is a single headed member of the myosin superfamily that localizes to the cytoplasm and the nucleus, where it is involved in transcription by RNA polymerases I and II, intranuclear transport, and nuclear export. In mammalian cells, three isoforms of myosin IC are expressed that differ only in the addition of short isoform-specific N-terminal peptides. Despite the high sequence homology, the isoforms show differences in cellular distribution, in localization to nuclear substructures, and in their interaction with nuclear proteins through yet unknown mechanisms. In this study, we used EGFP-fusion constructs that express truncated or mutated versions of myosin IC isoforms to detect regions that are involved in isoform-specific localization. We identified two nucleolar localization signals (NoLS). One NoLS is located in the myosin IC isoform B specific N-terminal peptide, the second NoLS is located upstream of the neck region within the head domain. We demonstrate that both NoLS are functional and necessary for nucleolar localization of specifically myosin IC isoform B. Our data provide a first mechanistic explanation for the observed functional differences between the myosin IC isoforms and are an important step toward our understanding of the underlying mechanisms that regulate the various and distinct functions of myosin IC isoforms.

Introduction

Myosin IC (formerly myosin Iβ) [1] is a member of the single headed class I myosins and localizes to the cytoplasm, the nucleus, and the nucleolus. In the cytoplasm, myosin IC associates with membranes and is involved in vesicle transport of membrane proteins [2], in regulation of the ion channels in the stereocilia of inner ear hair cells [3,4], and in the formation of membrane extensions in neuronal growth cones [5]. Besides its cytoplasmic role, myosin IC is also critically involved in nuclear processes. Myosin IC interacts with RNA polymerase I and RNA polymerase II and is involved in transcriptional processes [6–12]. It associates with RNA transcripts as well as pre-ribosomal and ribosomal units and is involved in their nuclear export [13,14]. Furthermore, together with actin, myosin IC acts as a molecular motor in intranuclear chromosome movements [15–17].

Until recently it was thought that the cytoplasmic and nuclear functions of myosin IC were facilitated by two isoforms; one

Abbreviations: NoLS, nucleolar localization signal; NMI, nuclear myosin I; NLS, nuclear localization signal; EGFP, enhanced green fluorescent protein; No, nucleolus; N, nucleus; C, cytoplasm; SV-40 TAg, simian virus 40 large T-antigen DAPI, 4′,6′-diamino-2-phenylindole; BSA, bovine serum albumin; SD, standard deviation; L2, loop 2 actin binding site; FC, fibrillar centre; DFC, dense fibrillar component; GC, granular component; aa, amino acids

**Corresponding author.* Fax: +1 716 829 2344.
E-mail address: whofmann@buffalo.edu (W.A. Hofmann).

[1] These authors contributed equally to this work.

0014-4827/$ - see front matter © 2013 Elsevier Inc. All rights reserved.
http://dx.doi.org/10.1016/j.yexcr.2013.02.008

isoform that localizes to the cytoplasm and a second isoform that contains a 16 amino acid long N-terminal peptide that localizes to the nucleus and was therefore called nuclear myosin I (NMI) [8,18]. However, a recent study identified the nuclear localization signal (NLS) of myosin IC within the neck domain of the protein, and thus in a region that is common among the myosin IC isoforms [19]. Furthermore, we recently showed that the *MYOIC* gene encodes not two, but three isoforms (myosin IC isoforms A, B, and C; [20]). The three isoforms differ only at their N-terminus by the addition of short N-terminal peptides that are encoded by specific upstream exons.

Myosin IC isoform C is the shortest isoform and does not contain an additional N-terminal peptide [21,22], isoform B (also known as nuclear myosin I; NMI) contains a 16 amino acid long N-terminal peptide [8], and isoform A contains a 35 amino acid long N-terminal peptide [20].

Interestingly, despite the sequence homology between the isoforms and the commonality of the NLS, the isoforms show differences in their nucleus to cytoplasm ratios, in their localization to nuclear substructures and in their interaction with nuclear proteins. Myosin IC isoform C shows a predominant localization to the cytoplasm [8,23,24]. Myosin IC isoforms A and B both localize to the nucleus but have differences in the ratios of nuclear to cytoplasmic distribution [20]. Furthermore, myosin IC isoforms A and B exhibit differences in their intranuclear localization and interaction with nuclear binding partners. Myosin IC Isoform B localizes to the nucleoplasm and nucleolus, interacts with RNA polymerases I and II and is critically involved in transcription by both RNA polymerases (reviewed in [25,26]). In contrast, myosin IC isoform A is absent from the nucleolus and does not interact with RNA polymerase I [20]. In addition, while both myosin IC isoforms interact in the nucleoplasm with RNA polymerase II, only isoform A but not isoform B associates with intranuclear speckles in a transcription dependent manner [20]. Taken together, these data suggest that the various myosin IC isoforms are functionally distinct. How these differences in localization and function are achieved however is unknown.

To gain a better understanding of the mechanisms that regulate cellular distribution of the myosin IC isoforms, we sought to identify the regions that are involved in intracellular localization. Here, we report the identification of the signals that target myosin IC to the nucleolus. We provide evidence of two functional nucleolar localization signals (NoLS) in myosin IC; one NoLS within the head domain and one NoLS within the isoform-specific N-terminal peptide of myosin IC isoform B. The identification of an isoform-specific intranuclear localization signal further underlines the emerging concept of functional differences between the myosin IC isoforms and provides a mechanistic explanation for the observed difference in cellular and specifically. intranuclear localization and function.

Materials and methods

Cell culture

COS-7 cells were purchased from ATCC and cultured in Dulbecco's modified Eagle's medium supplemented with 10% fetal bovine serum and 1% penicillin/streptomycin, at 37 °C with 5% CO_2.

Antibodies

Monoclonal anti-PolR1C antibody that recognizes RNA polymerase I was obtained from Sigma-Aldrich (St Louis, MO). Rabbit monoclonal anti-fibrillarin antibody and rabbit polyclonal anti-B23/nucleophosmin antibodies were purchased from Cell Signaling Inc. (C12C3; Danvers, MA) and from Santa Cruz Biotechnology Inc. (sc-6013-R; Santa Cruz, CA), respectively. Monoclonal mouse anti-β-actin antibodies and the rabbit polyclonal anti-NMI antibody that was raised against the 16 amino acid long N-terminal peptide of myosin IC isoform B (NMI) [6,8] were purchased from Sigma-Aldrich (St Louis, MO). The rabbit polyclonal anti-GFP antibody was obtained from Millipore (Billerica, MA). Secondary antibodies conjugated to texas red (TR) or peroxidase were obtained from Jackson ImmunoResearch Laboratories (West Grove, PA)

Plasmids and transfection

The various myosin IC fusion constructs are derivatives of myosin IC-EGFP isoform constructs [20]. To avoid confusion regarding the amino acid location of the various myosin IC domains, we adhered to the following numbering system of amino acids: the sequence that is common to all three isoforms starts with amino acid 1 to amino acid 1028. The additional N-terminal sequences of myosin IC isoforms A and B that are derived from upstream exons [8,20] are numbered B+1–B+16 for isoform B and A+1–A+35 for isoform A.

Point mutations in the coding sequence of myosin IC were generated using the QuickChange II Site-directed Mutagenesis Kit (Stratagene, La Jolla, CA, USA).

To obtain an expression vector of full length SV-40 large T-antigen (SV40-TAg) fused to EGFP at the C-terminus, total RNA was isolated from COS-7 cells using Trizol® reagent and reverse transcribed into cDNA using Superscript III reverse transcriptase (Invitrogen, Carlsbad, CA) following the manufacturer's instructions. Full length SV-40 TAg was then obtained by PCR and cloned into the pEGFP-N1 vector (Clontech Laboratories, Mountain View, CA).

For transfection experiments, COS-7 cells were plated on glass coverslips in 12 well plates (for immunocytochemistry) or in 6 well plates (for immunoblot analysis). 24 h later, the cells were transfected with 1 μg (12 well plate) or 3 μg (6 well plate) of the respective myosin IC constructs using Lipofectamine 2000 Reagent (Invitrogen, Carlsbad, CA). 20–48 h after transfection, cells were prepared for microscopic analysis or immunoblot analysis.

Immunocytochemistry and microscopy

For microscopic analysis, transfected cells were fixed with 4% paraformaldehyde for 15 min and coverslips were mounted with Prolong antifade containing 4′,6′-diamino-2-phenylindole (DAPI) (Invitrogen, Carlsbad, CA). For co-localization analysis, transfected cells grown on glass coverslips were fixed with 4% paraformaldehyde for 15 min, permeabilized with 0.1% Triton X-100, 0.1% Na-deoxycholate for 10 min, and then blocked with 5% BSA for 1 h. Incubations with the primary antibodies were conducted according to the manufacturers' protocols, followed by incubation for 1 h at room temperature with the appropriate secondary antibodies. Images were taken on a LSM 510 Meta confocal microscope (Carl Zeiss, Inc.) and processed using Photoshop (Adobe).

Cellular extract preparation and immunoblot analysis

To analyze expression of the various constructs, transfected cells were scraped from 6 well plates and lysed in SDS sample-buffer. Equal volumes of this crude cell extract were separated by 10% SDS-PAGE and transferred onto nitrocellulose membrane. After transfer, the nitrocellulose was probed with specific antibodies. The immunoreactive bands were detected by enhanced chemiluminescence. Expression of all constructs used in this study is shown in Supplementary Fig. S1.

Statistical analysis

For statistical analysis, at least 100 cells were counted in each of at least three independent experiments. Results are expressed as the mean ± SD and their significance was determined with a two-tailed student's *t*-test for pairwise comparison (significance level of $P<0.05$).

Results and discussion

Myosin IC, like all myosins, has a defined domain structure and is composed of a head, neck, and tail domain (Fig. 1A). The catalytic head domain contains the ATP- and actin-binding sites that are conserved among myosins [27,28]. The neck region contains three confirmed IQ domains to which regulatory calmodulin light chains bind [28]. This region also contains the recently identified NLS [19]. The C-terminal tail domain is assumed to facilitate interaction with specific binding partners [27,28]. In addition, two of the three myosin IC isoforms contain short N-terminal peptides with a length of 16 and 35 amino acids, respectively, with yet unknown functions (Fig. 1A) [8,20]. Interestingly, even though the three isoforms differ only in a very short N-terminal region, they show distinct cellular localizations. In general, isoform A localizes in the perinuclear region with some nuclear presence but a clear absence from nucleoli. Isoform B shows a strong nuclear and nucleolar localization, and isoform C shows a predominant cytoplasmic localization (Fig. 1B). This distribution of the myosin IC isoforms that is demonstrated here using myosin IC-EGFP fusion constructs, has been described and confirmed in previous studies using either fluorescently tagged proteins or isoform specific antibodies [6–8,18,20].

To identify domains of myosin IC that contribute to isoform-specific localization, we created a number of DNA constructs that express truncated versions of the myosin IC isoforms fused to EGFP at their C-terminus. These constructs were expressed in COS-7 cells and their localization was determined by confocal microscopy. Expression of all constructs used in this study was also confirmed by immunoblot (Supplementary Fig. S1).

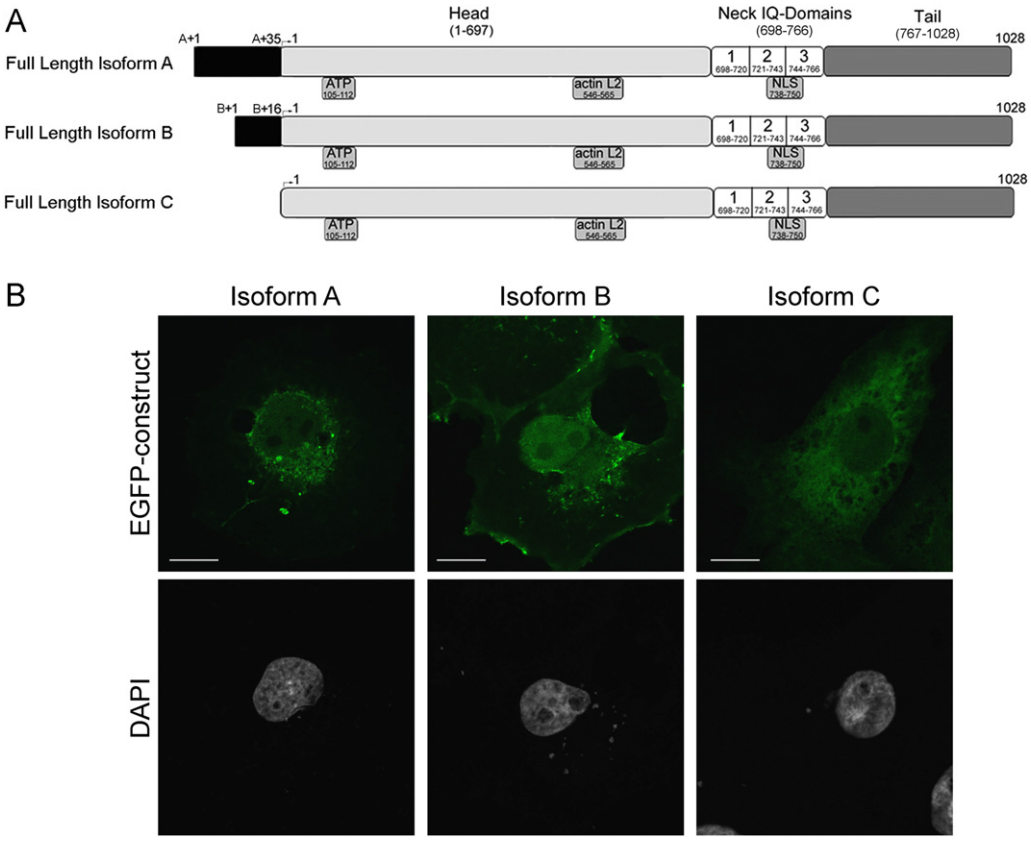

Fig. 1 – Expression of myosin IC-EGFP isoform constructs in COS-7 cells. (A) Schematic representation of the three myosin IC isoforms. Protein domains and regions of interest are indicated with their respective location. See Materials and Methods section for the rule applied to amino acid numbering of the various isoforms. (B) Representative confocal images of cells transfected with the indicated myosin IC-EGFP constructs. Note the differences in cellular localization between the three myosin IC isoforms. DAPI was used to visualize nuclei. Scale bar: 20 μm.

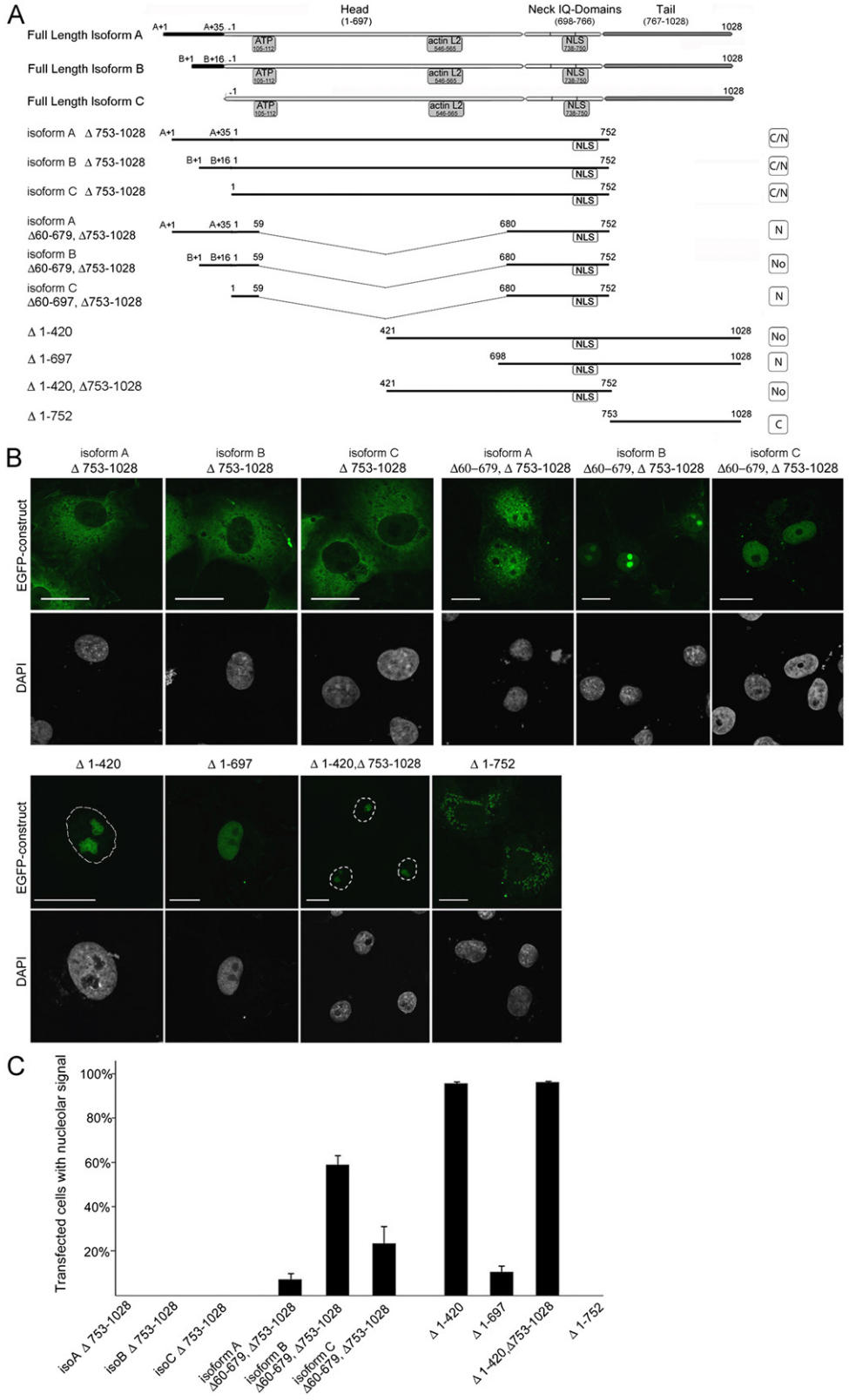

Fig. 2 – Identification of nucleolar localization signals in myosin IC isoform sequences. (A) Schematic representation of myosin IC full length and deletion constructs used to determine nucleolar localization of myosin IC isoforms. Protein domains and regions of interest are indicated. Cellular localization of constructs as shown in B and quantified in C is summarized on the right of the constructs. C = cytoplasm; N = nucleoplasm; No = Nucleolus. (B) Representative confocal images of cells transfected with the indicated myosin IC-EGFP constructs. DAPI was used to visualize nuclei. Scale bar: 20 μm. (C) Quantification of transfected cells that show a nucleolar signal. At least 100 cells were counted per experiment. Error bars = mean +SD; *n* = 3.

Identification of two NoLS; one in an isoform B-specific domain, one in a domain common to all isoforms

We started by analysing three constructs that contained the head domain with myosin IC isoform specific N-terminal regions and part of the IQ domain with the NLS, but were lacking the tail domain (Fig. 2A; isoform A Δ753–1028; isoform B Δ753–1028; isoform C Δ753–1028). However, even though all three constructs contain the IQ domain part with the recently identified NLS [19], none of these constructs showed a substantial nuclear localization (Fig. 2B). Because of the intrinsic property of the catalytic myosin head-domain to strongly bind to actin filaments, we considered the possibility that these constructs are retained in the cytoplasm through their interaction with actin filaments. Therefore, we deleted the ATP-binding site (Fig. 2A; ATP) and the ATP-dependent actin-binding site (Fig 2A, actin L2: loop 2 actin binding site located at the 50 kD:20 kD myosin head junction; [27,29]). The resulting three constructs contained the myosin IC isoform specific N-terminal regions, parts of the most N- and C-terminal region of the head domain, and the IQ domain with NLS (isoform A Δ60–679, Δ753–1028; isoform B Δ60–679, Δ753–1028; isoform C Δ60–679, Δ753–1028). As shown in Fig. 2B, deleting the ATP- and actin-binding sites had a considerable effect on the cellular localization of the constructs. All three constructs now show a substantial nuclear localization which confirmed our hypothesis that the intrinsic ATP/actin-binding of the head domain leads to retention in the cytoplasm.

Interestingly, while all three ATP/actin-binding site deletion constructs localized to the nucleus, they showed significant differences in their intranuclear distribution. The constructs that contain the myosin IC isoform A- and the isoform C-specific N-terminal regions localized to the nucleoplasm but were absent from the nucleolus in the majority of cells. In contrast, the construct that contained the myosin IC isoform B-specific N-terminal region accumulated strongly in the nucleolus (Fig. 2B and C).

The selective accumulation of the construct that contained the myosin IC isoform B-specific N-terminal peptide in the nucleolus correlates with the observed selective localization of the full length myosin IC isoform B-constructs and endogenous myosin IC isoform B to nucleoli (Fig. 1B) [20]. Because the three analysed constructs differ only in the isoform-specific N-terminal peptides, these data strongly suggest that the N-terminal peptides play an important role in the intranuclear distribution of the myosin IC isoforms. Specifically, our data indicate that the myosin IC isoform B-specific N-terminal peptide is involved in the translocation to or retention of this isoform in the nucleolus.

Tail domains of myosins are often involved in intracellular localization. Therefore, we also analysed constructs containing the tail region of myosin IC that is common to all myosin IC isoforms. The first construct had a deletion of amino acids 1–420 (including deletion of the N-terminal peptides) and only contained part of the head domain and the complete IQ and tail domains (Fig. 2B; Δ1–420). This construct showed almost exclusive nucleolar localization in over 95% of transfected cells which suggests that a second putative NoLS is present in a region that is common to all myosin IC isoforms.

To determine where exactly this second NoLS is located, we created a construct that contained the complete IQ and tail domains but no part of the head domain (Δ1–697) and a construct that contained the part of the head domain and the part of the IQ domain with the NLS but no tail domain (Δ1–697, Δ753–1028). As shown in Fig. 2B and C, the construct with the C-terminal head region but without the tail domain showed nucleolar localization. The construct missing the head region but containing the IQ- and tail-domains localized to the nucleoplasm but was absent from the nucleolus. This indicates that this second NoLS is located within the head domain. We also analysed a construct that contained part of IQ domain 3 and the complete tail domain (Δ1–753). This construct did not localize to the nucleus at all, confirming that nuclear localization is facilitated by the recently identified NLS that is located within IQ domains 2 and 3 [19].

Taken together, our analysis of myosin IC domains revealed the presence of two putative nucleolar localization signals. One NoLS is located in the head domain and therefore in an area that is common to all isoforms. The second NoLS is located in the myosin IC isoform B-specific N-terminal peptide and therefore specific to myosin IC isoform B. From here on we will call these two nucleolar localization signals $NoLS_{isoB}$ (myosin IC isoform B-specific NoLS) and $NoLS_H$ (NoLS within the head domain)

Identification of sequence elements in $NoLS_H$ that are involved in nucleolar localization

To confirm the functionality of each NoLS and to determine the sequence elements that facilitate nucleolar localization, we analysed each of the identified putative NoLS further.

As shown in Fig. 2, the construct that contains the part of the head domain between amino acids 421 and 698 (Fig. 2B) ($NoLS_H$) accumulates in the nucleolus in over 95% of transfected cells. To determine the minimally required amino acid sequence of $NoLS_H$ we created a number of sequential deletion constructs (Fig. 3A). Analysis of these constructs showed that the minimal sequence required for nucleolar localization is located between amino acids 619 and 637 (Fig. 3B and C). As indicated in the schematic representation (Fig. 3A), this 18 amino acid long sequence contains two clusters of basic amino acids ($R_{621}V_{622}R_{623}R_{624}$ and $R_{630}R_{631}K_{632}$). Because clusters of basic amino acids are common features of many NoLS [30], we further confirmed the functionality of this sequence for nucleolar localization by converting these two clusters of basic amino acids to alanines (Δ1–618, $R_{621,623,624}->A_{+621,623,624}$ and Δ1–618, $R_{630,631}K_{632}->A_{630-632}$). As shown in Fig. 3B and quantified in 3C, loss of either of the two clusters of basic amino acids resulted in the loss of nucleolar localization indicating that these basic amino acids within the identified minimal sequence are required for nucleolar localization.

In addition, we tested the nucleolar targeting potential of $NoLS_H$ by cloning the sequence coding for $NoLS_H$ (amino acids 619–730) upstream of the SV40 large T-antigen (SV40-TAg). SV40-TAg contains a classical NLS and localizes to the nucleus but not to the nucleolus [31] (Fig. 3B). Adding the sequence that codes for $NoLS_H$, leads to an accumulation of SV40-TAg in nucleoli. Removing the previously determined necessary amino acids 619 to 636 from this sequence abolishes nucleolar localization and restores the usual nuclear distribution of SV40-TAg (i.e., nuclear but not nucleolar) further confirming that $NoLS_H$ is indeed a nucleolar targeting signal.

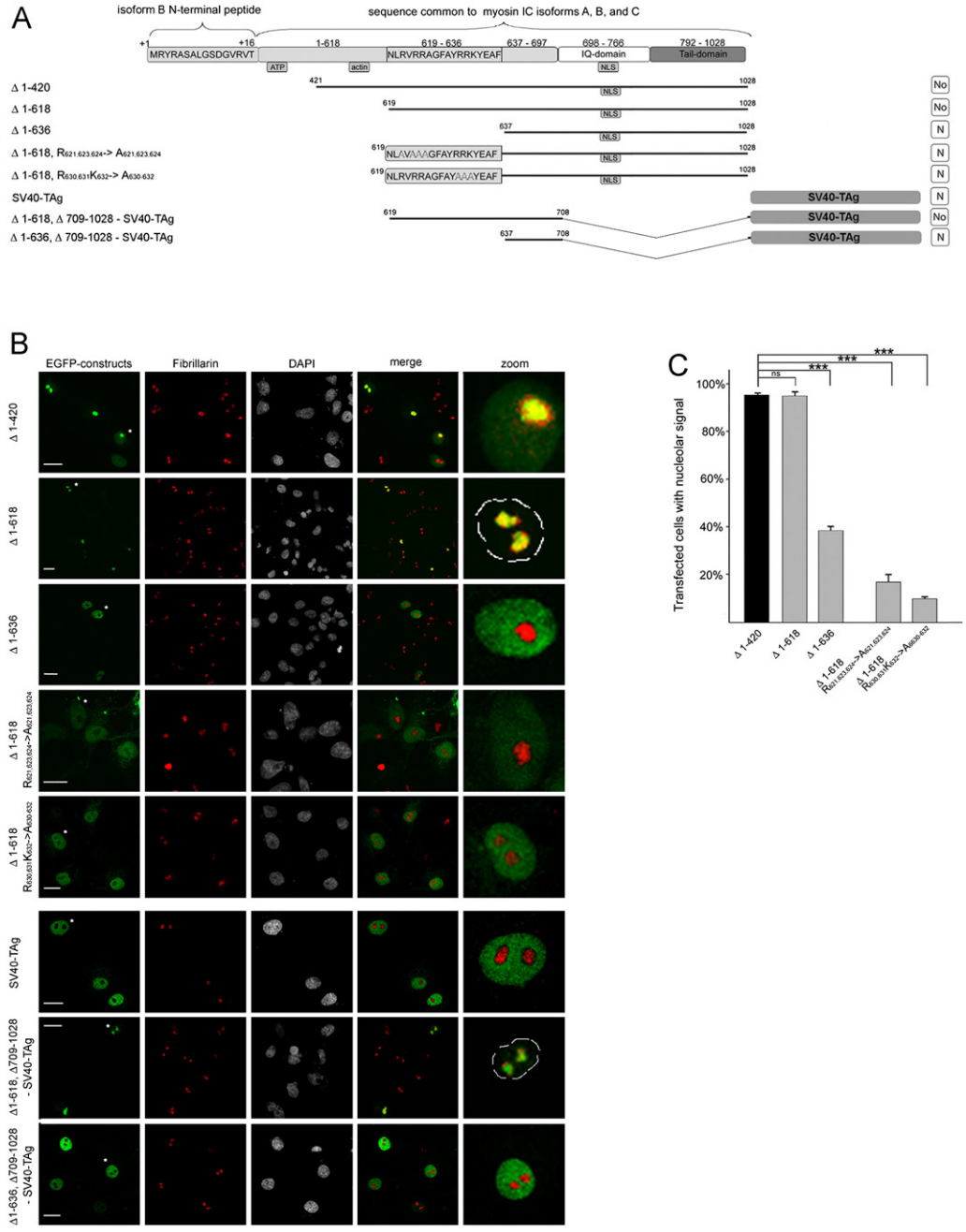

Fig. 3 – Identification of an NoLS in the myosin IC head domain. (A) Schematic representation of myosin IC wt, deletion, mutant, and SV-40TAg fusion constructs used to determine amino acids involved in nucleolar localization of myosin IC isoforms. Protein domains and regions of interest are indicated. Amino acids altered by site directed mutagenesis are represented in white. Localization of constructs as shown in B and quantified in C is summarized on the right of the constructs. N=nucleoplasm; No=Nucleolus. (B) Representative confocal images of cells transfected with the indicated myosin IC-or SV40-TAg-EGFP constructs and immunostained with anti-fibrillarin antibodies to mark nucleoli. DAPI was used to visualize nuclei. Right panel shows a merged and zoomed image of individual nuclei or nucleoli that are marked by a star in the left panel. Where appropriate, the outline of the nucleus is indicated in white. Scale bar: 20 μm. (C) Quantification of cells transfected with the indicated myosin IC-EGFP constructs that show a nucleolar signal. At least 100 cells were counted per experiment. Error bars=mean +SD; *n*=3. The significance in changes in nucleolar localization after deletion or site directed mutagenesis is indicated, *P* value=<0.05; ns= not significant, *=significant.**

NoLS$_H$ targets the myosin IC constructs to the granular component (GC)

Closer examination of the nucleolar localization of constructs that are targeted to the nucleolus through NoLS$_H$ revealed a distinct localization pattern that excludes certain nucleolar areas (Fig. 4A).

In higher eukaryotes the nucleolus is a highly organized structure that consists mainly of three functional compartments, i.e., fibrillar centre (FC), dense fibrillar component (DFC), and

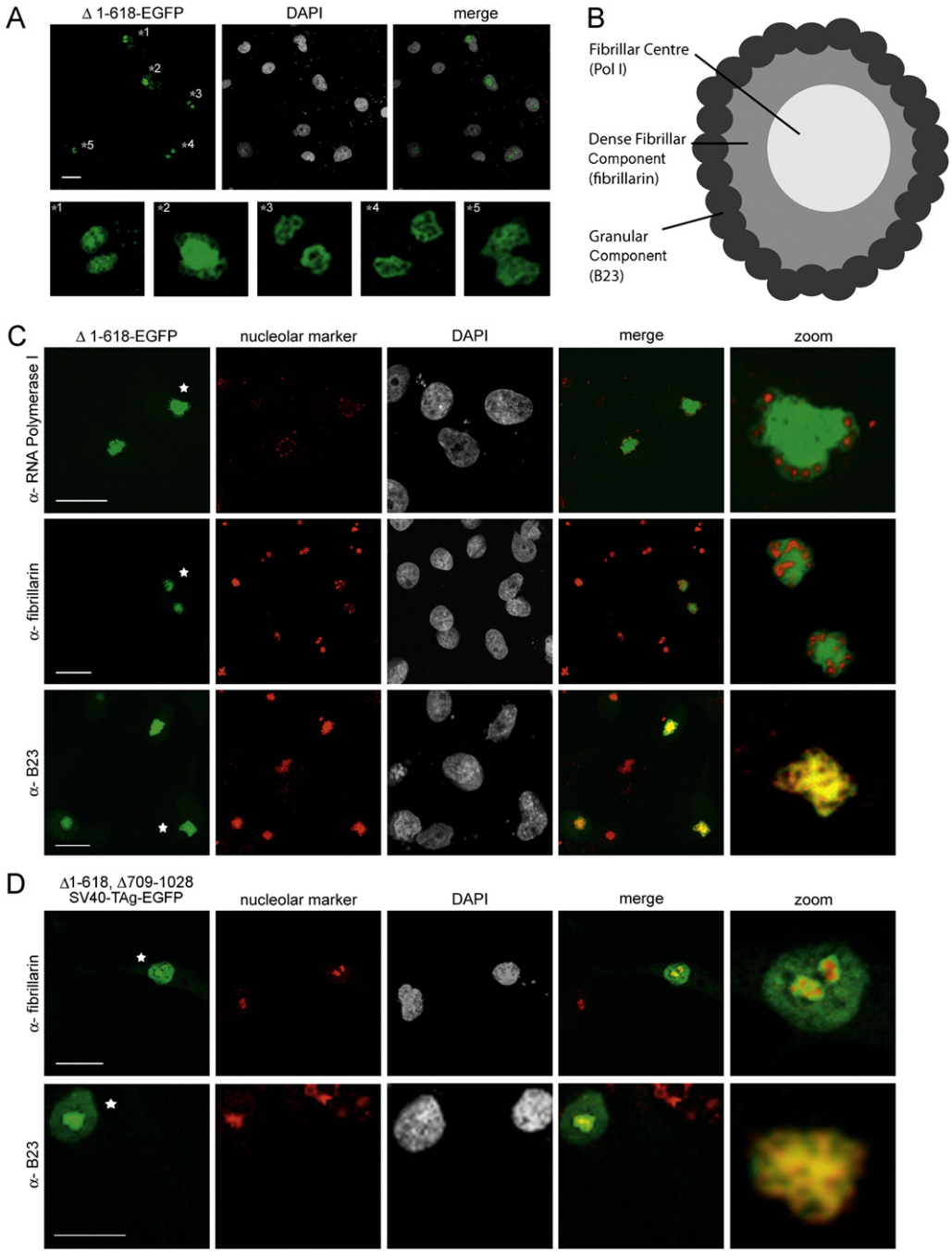

Fig. 4 – NoLS$_H$ targets myosin IC constructs to the granular component of the nucleolus. (A) Representative confocal microscopy image of cells transfected with Δ1–618-EGFP. DAPI was used to mark nuclei. Individual nucleoli from the wide field were each rescanned separately to adjust for variations in expression signals and are shown in magnified view below the wide field images Scale bar: 20 μm. (B) Schematic representation of nucleolar components and the marker proteins used to detect these. (C) Confocal microscopy images of co-localization between Δ1–618-EGFP construct and markers of nucleolar components. Cells transfected with the indicated constructs were fixed and stained with antibodies directed against RNA polymerase I, fibrillarin, and B23. DAPI was used to visualize nuclei. Right panel shows a merged and zoomed image of individual nucleoli that are marked by a star in the left panel. Scale bar: 20 μm.

granular component (GC) (schematic in Fig. 4B). The FC contains rDNA and components of the RNA polymerase I transcription machinery. Transcription of rRNA takes place in the FC and at the interface between FC and DFC; rRNA is processed in the DFC which is enriched in rRNA processing factors and pre-ribosome subunits are assembled in the GC [32,33].

To determine the nucleolar sub-structure the constructs localize to, we performed immunocolocalization studies. COS-7 cells transfected with Δ1–618-EGFP (NoLS$_H$; Fig. 4C) were analysed by immunostaining using antibodies directed against markers of nucleolar compartments. Specifically, we used antibodies directed against RNA polymerase I as a marker for FC, against

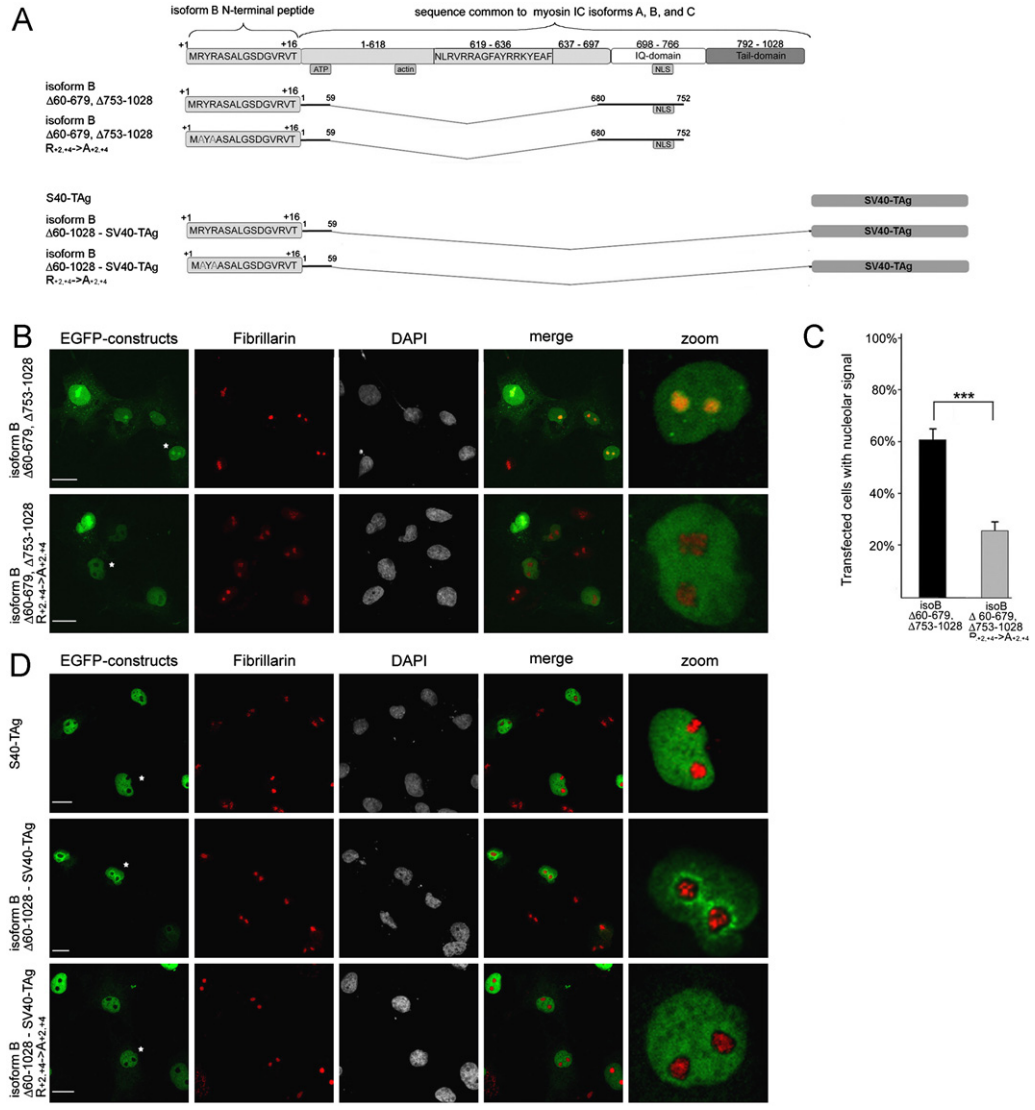

Fig. 5 – Identification of an NoLS in the myosin IC isoform specific N-terminal peptide. (A) Schematic representation of myosin IC isoform B wt, deletion, mutant and SV40-TAg fusion constructs used to determine amino acids involved in nucleolar localization of myosin IC isoforms. Localization of protein domains and regions of interest are indicated with their respective location. Amino acids altered by site directed mutagenesis are represented in white. (B) Representative confocal images of cells transfected with the indicated myosin IC-or SV40-TAG-EGFP constructs and immunostained with anti-fibrillarin antibodies to mark nucleoli. DAPI was used to visualize nuclei. Right panel shows a merged and zoomed image of individual nuclei or nucleoli that are marked by a star in the left panel. Scale bar: 20 μm. (C) Quantification of cells transfected with the indicated myosin IC-EGFP constructs that show a nucleolar signal. At least 100 cells were counted per experiment. Error bars = mean +SD; $n = 3$. The significance in changes in nucleolar localization after deletion or site directed mutagenesis is indicated, P value = < 0.05; ns = not significant, * = significant.**

fibrillarin as a marker for DFC, and against B23 as a marker for GC. Confocal analysis clearly shows that the constructs are absent from the FC and DFC. No co-localization is apparent with either RNA polymerase I or fibrillarin. However, we observed a co-localization with B23 which suggests that the constructs are targeted by $NoLS_H$ to the GC (Fig. 4B). Similar results were obtained analysing the localization of the SV40-TAg construct that is targeted to the nucleolus by $NoLS_H$. Here too the $NoLS_H$-SV40-TAg constructs co-localize with B23 but not with fibrillarin indicating a targeting of the SV40-TAg to the GC but not to FC or DFC (Fig. 4D).

Identification of sequence elements in $NoLS_{isoB}$ that are involved in nucleolar localization

The second putative NoLS ($NoLS_{isoB}$) we discovered through our analysis of the various myosin IC expression constructs appears to be located within the myosin IC isoform B-specific N-terminal peptide. As shown in Fig. 2, the construct that contains the myosin IC isoform B-specific N-terminal peptide (isoform B Δ60–679, Δ753–1028) shows nucleolar localization. In contrast, neither the construct that contains the myosin IC isoform A-specific N-terminal peptide (isoform A Δ60–679, Δ753–1028)

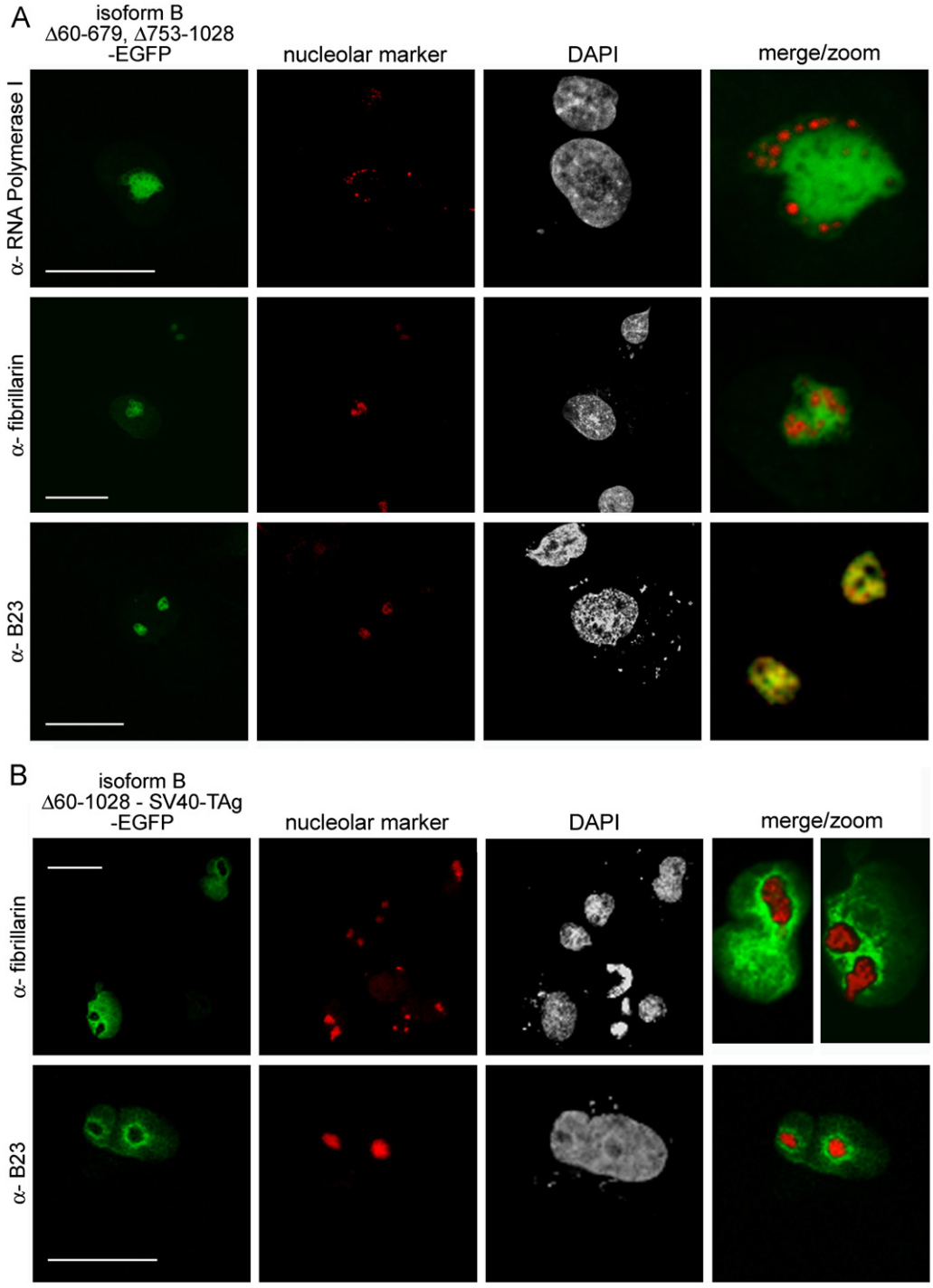

Fig. 6 – Analysis of $NoLS_{isoB}$ construct localization. (A) Confocal microscopy images of co-localization between isoform B Δ60–679, Δ753–1028-EGFP construct and markers of nucleolar components. Cells transfected with the indicated constructs were fixed and stained with antibodies directed against RNA polymerase I, fibrillarin, and B23. DAPI was used to visualize nuclei. Right panel shows a merged and zoomed image of individual nucleoli that are marked by a star in the left panel. Scale bar: 20 μm. (B) Confocal microscopy images of co-localization between isoform B Δ60–679, Δ753–1028-SV40-TAg-EGFP fusion constructs and markers of nucleolar components. Cells transfected with the indicated constructs were fixed and stained with antibodies directed against fibrillarin and B23. DAPI was used to visualize nuclei. Right panel shows a merged and zoomed image of individual nucleoli that are marked by a star in the left panel. Scale bar: 20 μm.

nor the myosin IC isoform C construct (isoform C Δ60–679, Δ753–1028) localizes to nucleoli in the majority of transfected cells. This suggests that nucleolar localization is facilitated through the myosin IC isoform B-specific 16 amino acid long N-terminal peptide ($NoLS_{isoB}$). We confirmed the importance of this peptide sequence for nucleolar localization by introducing

two point mutations using site directed mutagenesis (Fig. 5A). Specifically, we exchanged the two basic arginines at positions R_{+2} and R_{+4} for the nonpolar neutral amino acid alanine (Fig. 5A; isoB-Δ60–679, Δ753–1028, $R_{+2,+4}->A_{+2,+4}$). As shown in Fig. 5B and C, this substitution significantly decreases nucleolar localization from 61% to 23% of transfected cells. This strongly suggests that the myosin IC isoform B-specific N-terminal peptide constitutes a NoLS because either removing the peptide (which results in isoform C, Fig. 1A) or changing amino acids within the N-terminal peptide greatly reduces the number of cells in which nucleolar localization of the constructs can be observed.

Interestingly, when we cloned the sequence coding for $NoLS_{isoB}$ upstream of the SV40-TAg we observed a notable difference in nuclear and nucleolar localization when compared to the original $NoLS_{isoB}$-EGFP construct (Fig. 5D, middle row). As previously shown, SV40-TAg alone shows a ubiquitous distribution throughout the nucleoplasm with a clear absence from the nucleolus. Adding $NoLS_{isoB}$ leads to a strong accumulation not within but around the nucleolus. Importantly, this perinucleolar accumulation was not observed in cells transfected with the $NoLS_{isoB}$-SV40-TAg constructs in which the arginines at R_{+2} and R_{+4} of $NoLS_{isoB}$ were exchanged for alanines.

We next performed a more detailed analysis of the nucleolar localization patterns of the constructs containing $NoLS_{isoB}$. Similar to the constructs analysed in Figs. 3 and 4 that contain the $NoLS_H$ sequence, the constructs containing the N-terminal peptide of myosin IC isoform B plus the IQ domain parts of myosin IC with the NLS (isoform B Δ60–679, Δ753–1028) exhibit a distinct localization pattern that excludes certain nucleolar areas. Colocalization with nucleolar markers showed that these constructs are also absent from the FC and DFC but co-localize with B23, indicating a localization to the GC (Fig. 6B).

As shown in Fig. 5D, the localization pattern of the myosin IC isoform B-specific peptide fused to SV40-TAg differs from the isoform B Δ60–679,Δ753–1028 construct by exhibiting a perinucleolar rather than nucleolar localization. This was confirmed by co-localization experiments showing that the isoform B peptide-SV40-TAg fusion construct neither co-localizes with DFC nor GC components (Fig. 6B). Nonetheless, although intranucleolar localization cannot be observed, $NoLS_{isoB}$ does change the SV40-TAg localization from ubiquitous nucleoplasmic to perinucleolar indicating that $NoLS_{isoB}$ contains some form of nucleolar targeting capacity.

At this point we do not know what causes the different localization patterns of the two constructs containing $NoLS_{isoB}$. The myosin IC isoform B Δ60–679, Δ753–1028 construct that localizes to the GC is relatively small in size with a molecular weight of ~45 kD while the isoform B peptide-SV40-TAg-EGFP fusion protein has a substantially larger size of ~120 kD (Supplementary Fig. S1). However, the construct containing the myosin IC isoform A specific peptide is only 20 aa larger while the myosin IC isoform C specific N-terminal region is even 19 aa shorter compared to myosin IC isoform B Δ60–679, Δ753–1028 (Fig. 2A). Yet, there is a substantial difference in nucleolar localization between the three constructs (Fig. 2C). In addition, nucleolar localization of myosin IC isoform B Δ60–679, Δ753–1028 construct was significantly decreased by introducing specific point mutations in the myosin IC isoform B specific peptide sequence (Fig. 5B). Taken together, this strongly suggests that nucleolar targeting is indeed facilitated by the isoform B specific peptide sequence. Unclear is the exact target locus, i.e., perinucleolar region or GC and further studies are needed to determine why there is a difference in the specific nucleolar/perinucleolar localization between the myosin IC isoform B Δ60–679, Δ753–1028 and the isoform B peptide-SV40-TAg-EGFP fusion proteins.

Functional studies on the role of myosin IC isoform B (NMI) in RNA polymerase I transcription showed that myosin IC isoform B is in complex with RNA polymerase I, involved in the assembly of TIF transcription complexes, and associates with rDNA [9,10,20]. Furthermore, myosin IC isoform B associates with the B-WICH chromatin remodelling complex and a role in rRNA transcription elongation has been proposed [11]. Accordingly, nucleolar localization studies showed myosin IC isoform B at nucleolar organization regions in the FC and DFC [6]. In addition, a recent study analysing intranuclear translocations of myosin IC isoform B in response to changes in transcriptional activity demonstrated that in transcriptionally inactive nuclei isoform B predominantly localizes to the DFC while upon activation of rRNA transcription, an increase of isoform B in the DFC and GC was observed [12,34]. The fact that we did not observe a localization of the EGFP tagged constructs to either FC or DFC but an almost exclusive localization to the GC and, in case of the $NoLS_{isoB}$-SV40-TAg fusion, to perinucleolar regions, suggests that a complex interaction with nucleolar components is involved in localization and function of myosin IC isoform B. While the identified $NoLS_{isoB}$ seem to target isoform B to perinucleolar regions and $NoLS_H$ to the GC component of the nucleolus, further interactions are presumably required to facilitate translocation of myosin IC isoform B to the place of active transcription. Because we only used partial constructs for our analysis so far, it is probable that elements that are involved in binding of such nucleolar components might be missing and further studies are needed to determine the precise interactions of myosin IC isoform B with nucleolar components.

$NoLS_H$ and $NoLS_{isoB}$ are both necessary for nucleolar localization of myosin IC isoform B

Our analysis so far showed that both identified nucleolar localization signals are functional in that they both have the potential to localize proteins and peptides to the nucleolus or into the vicinity of the nucleolus. To determine if one or both NoLS are actually functionally involved in localizing full length myosin IC isoform B to the nucleolus, we introduced the point mutations that have been shown to inactivate $NoLS_H$ (Fig. 3) and $NoLS_{isoB}$ (Fig. 5) into full length myosin IC isoform B-EGFP (Fig. 7A). Analysis of these constructs by confocal microscopy showed that mutating either $NoLS_{isoB}$ or $NoLS_H$ prevented myosin IC isoform B from localizing to the nucleolus. This suggests that both NoLS are required for the nucleolar localization of the full length protein. The necessity of both NoLS for nucleolar localization might also explain why myosin IC isoforms A and C do not show nucleolar localization even though they do contain the sequence for $NoLS_H$ (Fig. 1) [20].

In this context it is interesting to note that even though $NoLS_H$ and $NoLS_{isoB}$ seem to be independently able to target peptides or non-myosin proteins towards the nucleolus, they show substantial differences in their efficiency. $NoLS_H$ has a very high

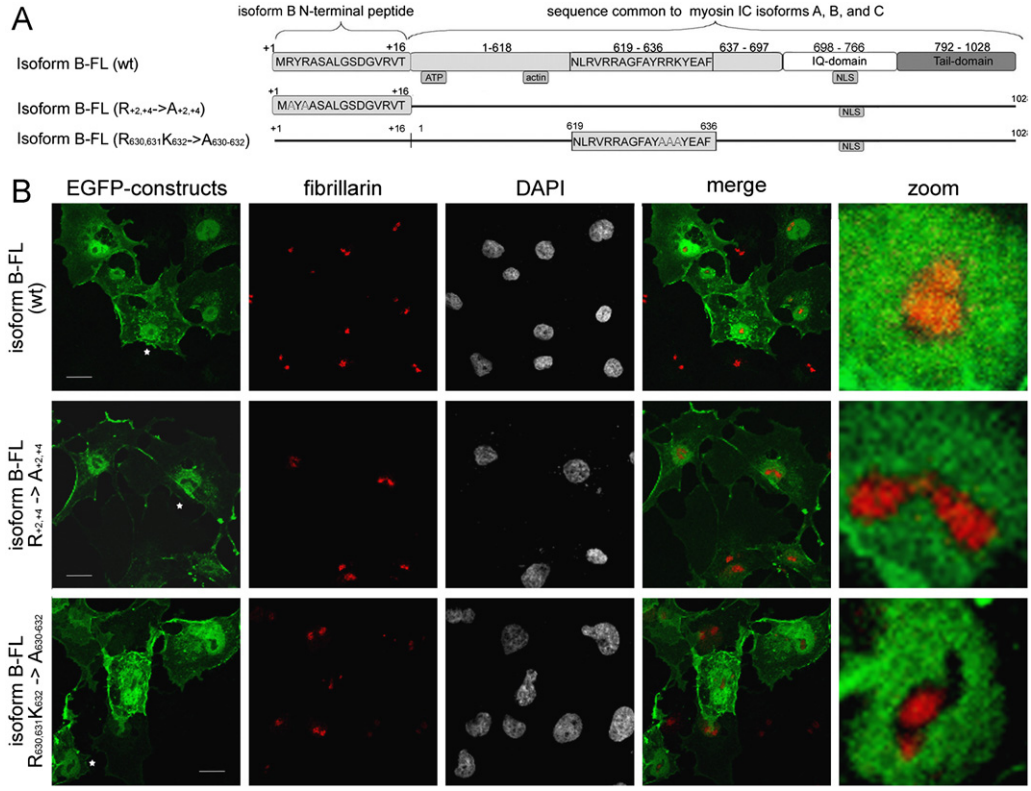

Fig. 7 – $NoLS_H$ and $NoLS_{isoB}$ are both necessary for nucleolar localization of full length myosin IC isoform B. (A) Schematic representation of myosin IC isoform B wt and mutant constructs used. Amino acid sequences of interest are indicated. Amino acids altered by site directed mutagenesis are represented in white. (B) Representative confocal images of cells transfected with the indicated myosin IC-EGFP constructs. Cells transfected with the indicated constructs were fixed and stained with antibodies directed against fibrillarin as a marker for nucleoli. DAPI was used to visualize nuclei. Right panel shows a merged and zoomed image of individual nucleoli that are marked by a star in the left panel. Scale bar: 20 μm.

efficiency and targets the expressed constructs almost completely to the nucleolus in over 95% of transfected cells. In contrast, the NoLS that is specific to the N-terminal peptide of myosin IC isoform B ($NoLS_{isoB}$) seems to be less efficient and only in 61% of transfected cells nucleolar localization is observed in addition to nucleoplasmic localization. In addition, $NoLS_{isoB}$ did not target SV40-TAg into the nucleolus but rather lead to a perinucleolar accumulation. Nonetheless, considering that myosin IC isoforms A and C do contain $NoLS_H$ but do not localize to the nucleolus, it is reasonable to assume that $NoLS_{isoB}$ is the primary signal that targets myosin IC to the nucleolus. The presence of multiple signals that contribute in varying levels to the overall localization of a protein has been described previously for nucleolar as well as for nuclear localization signals [35–38]. However, in most cases it is unclear why multiple signals are needed. In case of myosin IC, the presence of multiple NoLS could ensure that nucleolar localization is both, isoform specific and efficient. Nucleolar localization signals are usually located in easily accessible areas at the surface of proteins and nucleolar retention is thought to be predominantly mediated through functional interaction with nucleolar core components [30,39,40]. Although there is no crystal structure of the head domain of myosin IC available, it is expected that the myosin IC head assumes the general conformation as other myosin head domains. Thus, resolved three dimensional structures of myosin II head domains can be used for comparison [27,28,41,42]. Interestingly, according to these crystal structures [42,43], the most N-terminal amino acids of the head domain are free and easily accessible. In contrast, $NoLS_H$ is located in the hinge region between the head and neck domain in an area that undergoes substantial alterations depending on nucleotide-, actin- and light chain binding. We therefore propose the hypothesis that after some of the nuclear myosin IC isoform B has been targeted to the nucleolus or at least to a perinucleolar region through the easily accessible $NoLS_{isoB}$, the region around $NoLS_H$ undergoes structural changes after interacting with nucleolar binding partners. This interaction then exposes $NoLS_H$ which in turn strengthen the retention of myosin IC isoform B in the nucleolus. While we currently do not have experimental data to prove this hypothesis, it represents an attractive model that would explain the isoform specific localization of myosin IC to the nucleolus, even though only one of the identified NoLS is isoform specific, while the second NoLS is common to all myosin IC isoforms.

In this context, the previously reported calmodulin-sensitive nuclear translocation of myosin IC might be of interest [19]. Calmodulin is the regulatory light chain of myosin IC and calmodulin binding to the neck is one of the mechanisms that could lead to structural changes in the above mentioned hinge region between the head and neck domain that might alter accessibility of $NoLS_H$. However, if indeed calmodulin-binding, the interaction with nuclear actin, or yet another regulatory mechanism is involved in nucleolar translocation and in the

facilitation of the multiple nucleolar functions of myosin IC isoform B, remains to be determined.

In conclusion, we have identified two functional localization signals that facilitate specifically the nucleolar localization of myosin IC isoform B. Previous studies indicated that the various myosin IC isoforms have distinct functions in the nucleus and we now present a mechanistic explanation of these functional differences. This study provides first evidence for a functionality of the isoform specific N-terminal peptides in facilitating translocation to specific cellular compartments.

Acknowledgments

We acknowledge Undergraduate Research Awards from the University at Buffalo, Center for Undergraduate Research & Creative Activities (CURCA) to R.S.S. and S.Z.S.A.Y. This study was funded in part by the Department of Defense CDMRP (PC111523 to W.A.H.)

Appendix A. Supporting information

Supplementary data associated with this article can be found in the online version at http://dx.doi.org/10.1016/j.yexcr.2013.02.008.

REFERENCES

[1] P.G. Gillespie, J.P. Albanesi, M. Bahler, W.M. Bement, J.S. Berg, D.R. Burgess, B. Burnside, R.E. Cheney, D.P. Corey, E. Coudrier, P. de Lanerolle, J.A. Hammer, T. Hasson, J.R. Holt, A.J. Hudspeth, M. Ikebe, J. Kendrick-Jones, E.D. Korn, R. Li, J.A. Mercer, R.A. Milligan, M.S. Mooseker, E.M. Ostap, C. Petit, T.D. Pollard, J.R. Sellers, T. Soldati, M.A. Titus, Myosin-I nomenclature, J. Cell Biol. 155 (2001) 703–704.

[2] A. Bose, A. Guilherme, S.I. Robida, S.M. Nicoloro, Q.L. Zhou, Z.Y. Jiang, D.P. Pomerleau, M.P. Czech, Glucose transporter recycling in response to insulin is facilitated by myosin Myo1c, Nature 420 (2002) 821–824.

[3] J.L. Cyr, R.A. Dumont, P.G. Gillespie, Myosin-1c interacts with hair-cell receptors through its calmodulin-binding IQ domains, J. Neurosci. 22 (2002) 2487–2495.

[4] J.R. Holt, S.K. Gillespie, D.W. Provance, K. Shah, K.M. Shokat, D.P. Corey, J.A. Mercer, P.G. Gillespie, A chemical-genetic strategy implicates myosin-1c in adaptation by hair cells, Cell 108 (2002) 371–381.

[5] F.S. Wang, C.W. Liu, T.J. Diefenbach, D.G. Jay, Modeling the role of myosin 1c in neuronal growth cone turning, Biophys. J. 85 (2003) 3319–3328.

[6] N. Fomproix, P. Percipalle, An actin-myosin complex on actively transcribing genes, Exp. Cell Res. 294 (2004) 140–148.

[7] W.A. Hofmann, G.M. Vargas, R. Ramchandran, L. Stojiljkovic, J.A. Goodrich, P. de Lanerolle, Nuclear myosin I is necessary for the formation of the first phosphodiester bond during transcription initiation by RNA polymerase II, J. Cell. Biochem. 99 (2006) 1001–1009.

[8] L. Pestic-Dragovich, L. Stojiljkovic, A.A. Philimonenko, G. Nowak, Y. Ke, R.E. Settlage, J. Shabanowitz, D.F. Hunt, P. Hozak, P. de Lanerolle, A myosin I isoform in the nucleus, Science 290 (2000) 337–341.

[9] V.V. Philimonenko, J. Zhao, S. Iben, H. Dingova, K. Kysela, M. Kahle, H. Zentgraf, W.A. Hofmann, P. de Lanerolle, P. Hozak, I. Grummt, Nuclear actin and myosin I are required for RNA polymerase I transcription, Nat. Cell Biol. 6 (2004) 1165–1172.

[10] J. Ye, J. Zhao, U. Hoffmann-Rohrer, I. Grummt, Nuclear myosin I acts in concert with polymeric actin to drive RNA polymerase I transcription, Genes Dev. 22 (2008) 322–330.

[11] P. Percipalle, N. Fomproix, E. Cavellan, R. Voit, G. Reimer, T. Kruger, J. Thyberg, U. Scheer, I. Grummt, A.K. Farrants, The chromatin remodelling complex WSTF-SNF2h interacts with nuclear myosin 1 and has a role in RNA polymerase I transcription, EMBO Rep. 7 (2006) 525–530.

[12] K. Kysela, A.A. Philimonenko, V.V. Philimonenko, J. Janacek, M. Kahle, P. Hozak, Nuclear distribution of actin and myosin I depends on transcriptional activity of the cell, Histochem. Cell Biol. 124 (2005) 347–358.

[13] B. Cisterna, D. Necchi, E. Prosperi, M. Biggiogera, Small ribosomal subunits associate with nuclear myosin and actin in transit to the nuclear pores, FASEB J. 20 (2006) 1901–1903.

[14] A. Obrdlik, E. Louvet, A. Kukalev, D. Naschekin, E. Kiseleva, B. Fahrenkrog, P. Percipalle, Nuclear myosin 1 is in complex with mature rRNA transcripts and associates with the nuclear pore basket, FASEB J. 24 (2010) 146–157.

[15] C.H. Chuang, A.E. Carpenter, B. Fuchsova, T. Johnson, P. de Lanerolle, A.S. Belmont, Long-range directional movement of an interphase chromosome site, Curr. Biol. 16 (2006) 825–831.

[16] Q. Hu, Y.S. Kwon, E. Nunez, M.D. Cardamone, K.R. Hutt, K.A. Ohgi, I. Garcia-Bassets, D.W. Rose, C.K. Glass, M.G. Rosenfeld, X.D. Fu, Enhancing nuclear receptor-induced transcription requires nuclear motor and LSD1-dependent gene networking in interchromatin granules, Proc. Nat. Acad. Sci. U.S.A. 105 (2008) 19199–19204.

[17] I.S. Mehta, L.S. Elcock, M. Amira, I.R. Kill, J.M. Bridger, Nuclear motors and nuclear structures containing A-type lamins and emerin: is there a functional link?, Biochem. Soc. Trans. 36 (2008) 1384–1388.

[18] G. Nowak, L. Pestic-Dragovich, P. Hozak, A. Philimonenko, C. Simerly, G. Schatten, P. de Lanerolle, Evidence for the presence of myosin I in the nucleus, J. Biol. Chem. 272 (1997) 17176–17181.

[19] R. Dzijak, S. Yildirim, M. Kahle, P. Novak, J. Hnilicova, T. Venit, P. Hozak, Specific nuclear localizing sequence directs two myosin isoforms to the cell nucleus in calmodulin-sensitive manner, PLoS One 7 (2012) e30529.

[20] I. Ihnatovych, M. Migocka-Patrzalek, M. Dukh, W.A. Hofmann, Identification and characterization of a novel myosin Ic isoform that localizes to the nucleus, Cytoskeleton (Hoboken) 69 (2012) 555–565.

[21] E.H. Sherr, M.P. Joyce, L.A. Greene, Mammalian myosin I alpha, I beta, and I gamma: new widely expressed genes of the myosin I family, J. Cell Biol. 120 (1993) 1405–1416.

[22] O. Reizes, B. Barylko, C. Li, T.C. Sudhof, J.P. Albanesi, Domain structure of a mammalian myosin I beta, Proc. Nat. Acad. Sci. U.S.A. 91 (1994) 6349–6353.

[23] M.C. Wagner, B.A. Molitoris, ATP depletion alters myosin I beta cellular location in LLC-PK1 cells, Am. J. Physiol. 272 (1997) C1680–C1690.

[24] I.C. Baines, H. Brzeska, E.D. Korn, Differential localization of Acanthamoeba myosin I isoforms, J. Cell Biol. 119 (1992) 1193–1203.

[25] P. de Lanerolle, T. Johnson, W.A. Hofmann, Actin and myosin I in the nucleus: what next?, Nat. Struct. Mol. Biol. 12 (2005) 742–746.

[26] C. Erlinger, H. Lettner, A. Hubmer, W. Hofmann, F. Steinhausler, Determination of (137)Cs in the water system of a pre-Alpine lake, J. Environ. Radioact. 100 (2009) 354–360.

[27] M.S. Mooseker, R.E. Cheney, Unconventional myosins, Annu. Rev. Cell Dev. Biol. 11 (1995) 633–675.

[28] B. Barylko, G. Jung, J.P. Albanesi, Structure, function, and regulation of myosin 1C, Acta Biochim. Pol. 52 (2005) 373–380.

[29] I. Rayment, H.M. Holden, M. Whittaker, C.B. Yohn, M. Lorenz, K.C. Holmes, R.A. Milligan, Structure of the actin-myosin complex and its implications for muscle contraction, Science 261 (1993) 58–65.
[30] M.S. Scott, F.M. Boisvert, M.D. McDowall, A.I. Lamond, G.J. Barton, Characterization and prediction of protein nucleolar localization sequences, Nucleic Acids Res. 38 (2010) 7388–7399.
[31] D. Kalderon, B.L. Roberts, W.D. Richardson, A.E. Smith, A short amino acid sequence able to specify nuclear location, Cell 39 (1984) 499–509.
[32] F.M. Boisvert, S. van Koningsbruggen, J. Navascues, A.I. Lamond, The multifunctional nucleolus, Nature reviews, J. Mol. Cell. Biol. 8 (2007) 574–585.
[33] T. Pederson, The nucleolus, Cold Spring Harbor Perspect. Biol. 3 (2011).
[34] V.V. Philimonenko, J. Janacek, M. Harata, P. Hozak, Transcription-dependent rearrangements of actin and nuclear myosin I in the nucleolus, Histochem. Cell Biol. 134 (2010) 243–249.
[35] I. Kalt, A. Levy, T. Borodianskiy-Shteinberg, R. Sarid, Nucleolar localization of GLTSCR2/PICT-1 is mediated by multiple unique nucleolar localization sequences, PLoS One 7 (2012) e30825.
[36] G. Zhou, C.L. Doci, M.W. Lingen, Identification and functional analysis of NOL7 nuclear and nucleolar localization signals, BMC Cell Biol. 11 (2010) 74.
[37] M.A. Hahn, D.J. Marsh, Nucleolar localization of parafibromin is mediated by three nucleolar localization signals, FEBS Lett. 581 (2007) 5070–5074.
[38] L.J. Terry, E.B. Shows, S.R. Wente, Crossing the nuclear envelope: hierarchical regulation of nucleocytoplasmic transport, Science 318 (2007) 1412–1416.
[39] E. Emmott, J.A. Hiscox, Nucleolar targeting: the hub of the matter, EMBO Rep. 10 (2009) 231–238.
[40] I. Raska, P.J. Shaw, D. Cmarko, New insights into nucleolar architecture and activity, Int. Rev. Cytol. 255 (2006) 177–235.
[41] M.A. Hartman, D. Finan, S. Sivaramakrishnan, J.A. Spudich, Principles of unconventional myosin function and targeting, Annu. Rev. Cell Dev. Biol. 27 (2011) 133–155.
[42] W. Kliche, S. Fujita-Becker, M. Kollmar, D.J. Manstein, F.J. Kull, Structure of a genetically engineered molecular motor, EMBO J. 20 (2001) 40–46.
[43] I. Rayment, W.R. Rypniewski, K. Schmidt-Base, R. Smith, D.R. Tomchick, M.M. Benning, D.A. Winkelmann, G. Wesenberg, H.M. Holden, Three-dimensional structure of myosin subfragment-1: a molecular motor, Science 261 (1993) 50–58.

Lamin A tail modification by SUMO1 is disrupted by familial partial lipodystrophy–causing mutations

Dan N. Simon[a], Tera Domaradzki[b], Wilma A. Hofmann[b], and Katherine L. Wilson[a]
[a]Department of Cell Biology, Johns Hopkins University School of Medicine, Baltimore, MD 21205; [b]Department of Physiology and Biophysics, University at Buffalo-State University of New York, Buffalo, NY 14214

ABSTRACT **Lamin filaments are major components of the nucleoskeleton that bind LINC complexes and many nuclear membrane proteins. The tail domain of lamin A directly binds 21 known partners, including actin, emerin, and SREBP1, but how these interactions are regulated is unknown. We report small ubiquitin-like modifier 1 (SUMO1) as a major new post-translational modification of the lamin A tail. Two SUMO1 modification sites were identified based on in vitro SUMOylation assays and studies of Cos-7 cells. One site (K420) matches the SUMO1 target consensus; the other (K486) does not. On the basis of the position of K486 on the lamin A Ig-fold, we hypothesize the SUMO1 E2 enzyme recognizes a folded structure–dependent motif that includes residues genetically linked to familial partial lipodystrophy (FPLD). Supporting this model, SUMO1-modification of the lamin A tail is reduced by two FPLD-causing mutations, G465D and K486N, and by single mutations in acidic residues E460 and D461. These results suggest a novel mode of functional control over lamin A in cells.**

Monitoring Editor
Robert D. Goldman
Northwestern University

Received: Jul 18, 2012
Revised: Nov 28, 2012
Accepted: Dec 4, 2012

INTRODUCTION

The small ubiquitin-like modifier (SUMO) family consists of four conserved ~10-kDa proteins (SUMO1, SUMO2, SUMO3, SUMO4) that are covalently and reversibly attached to lysine residues on target proteins (Gareau and Lima, 2010). SUMOylation can regulate the localization, function, and interactions of target proteins and influences many cellular pathways, including nuclear import/export, transcription, apoptosis, cell cycle regulation, and protein stability (Geiss-Friedlander and Melchior, 2007). At the molecular level, SUMOylation can block binding to specific partners, confer binding to new partners bearing a "SUMO interaction motif" (SIM), or change protein conformation (Wilkinson and Henley, 2010). The enzymes responsible for SUMO conjugation, and many SUMOylated proteins, are located primarily in the nucleus (Gareau and Lima, 2010). For example, actin, a major component of the nucleoskeleton (Visa and Percipalle, 2010; Simon and Wilson, 2011), is modified by SUMO2 and SUMO3 as a mechanism for retention in the nucleus (Hofmann *et al.*, 2009). Another nucleoskeletal protein, lamin A, is modified by SUMO2 (Zhang and Sarge, 2008).

Nuclear intermediate filaments formed by A- and B-type lamins are major components of the nucleoskeleton and are responsible for nuclear shape, assembly, and genome tethering (Dittmer and Misteli, 2011; Simon and Wilson, 2011; Gerace and Huber, 2012). Lamins also bind signaling and chromatin-regulatory proteins, support epigenetic regulation, and are involved in mechanotransduction, development, transcription, replication, and DNA-damage repair (Dechat *et al.*, 2008; Wilson and Berk, 2010; Wilson and Foisner, 2010). In mammalian cells, *LMNB1* and *LMNB2* encode somatic lamins B1 and B2, respectively; *LMNB2* also encodes the spermatocyte-specific lamin B3 (Dittmer and Misteli, 2011). Together B-type lamins are essential for embryogenesis in mice (Kim *et al.*, 2011b), with distinct contributions to the developing brain (Takamori *et al.*, 2007; Coffinier *et al.*, 2010, 2011). The mammalian *LMNA* gene is alternatively spliced to generate somatic lamins A and C (and minor isoform AΔ10) and spermatocyte-specific lamin C2 (Dittmer and Misteli, 2011). The A-type lamins are not essential at the cellular level but influence many specific tissues during development (Dechat *et al.*, 2010a; Dittmer and Misteli, 2011; Gerace and Huber,

This article was published online ahead of print in MBoC in Press (http://www.molbiolcell.org/cgi/doi/10.1091/mbc.E12-07-0527) on December 14, 2012.

Address correspondence to: Katherine L. Wilson (klwilson@jhmi.edu), Wilma A. Hofmann (whofmann@buffalo.edu).

Abbreviations used: FPLD, familial partial lipodystrophy; GFP, green fluorescent protein; GST, glutatione *S*-transferase; HGPS, Hutchinson-Gilford progeria syndrome; LINC, links the nucleoskeleton and cytoskeleton; SIM, SUMO interaction motif; SREBP1, sterol response element binding protein 1; SUMO, small ubiquitin-like modifier.

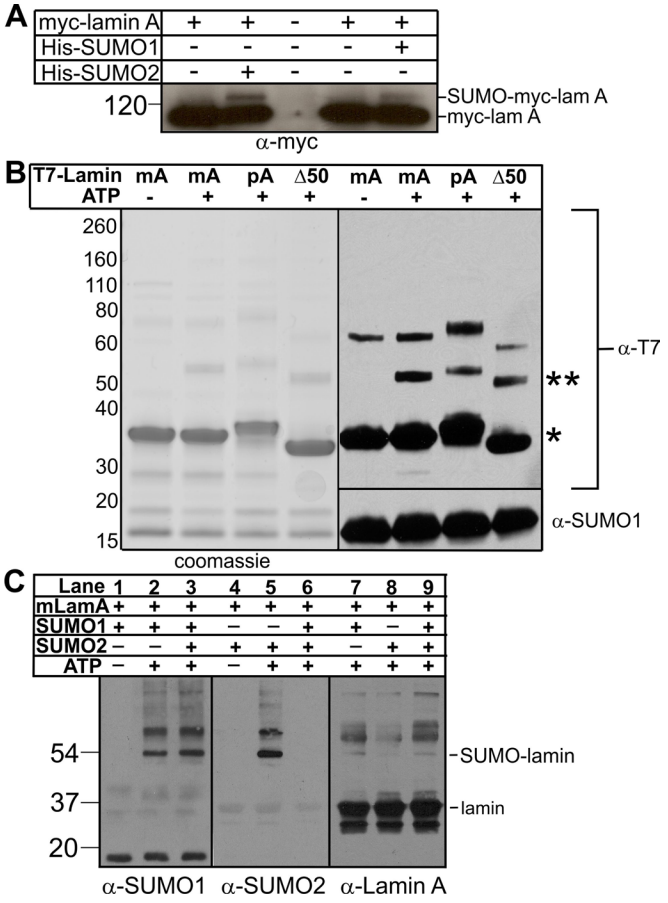

FIGURE 1: Modification of lamin A by SUMO1 or SUMO2 in vitro and in Cos-7 cells. (A) Exogenous mature myc-lamin A is modified by SUMO1 and SUMO2. Cos-7 cells were transfected to express the indicated constructs for 36 h, then lysed, incubated with Ni^{2+} beads to recover His-SUMO and lamin A (which has a natural His tag), resolved by SDS–PAGE, and immunoblotted with antibodies to myc (α-myc); $n = 3$. (B) Recombinant purified mature (mA), precursor (pA), or Δ50 (Δ50) lamin A tail-domain polypeptides were incubated with SUMO1, E1, and E2 with or without ATP for 3 h at 30°C. Reactions were resolved by SDS–PAGE in duplicate and either stained with Coomassie blue or immunoblotted first with antibodies to the T7 tag (α-T7) and then stripped and reprobed with antibodies to SUMO1 (α-SUMO1); $n = 3$. Unmodified lamin A tails are marked by an asterisk and SUMO1-modified lamin A tails by a double asterisk. (C) Mature lamin A tails were incubated with either SUMO1 or SUMO2 (or both) along with E1, E2, and ATP for 1 h at 30°C and then immunoblotted with antibodies specific for SUMO1 (α-SUMO1), SUMO2 (α-SUMO2), or lamin A tail (α-Lamin A); $n = 3$.

2012), with particular roles in mechanosensitive gene expression (Lammerding *et al.*, 2004) and pRb-dependent cell proliferation control (Dechat *et al.*, 2010b). Mutations in *LMNA* cause at least 15 tissue-specific diseases (laminopathies), including Emery–Dreifuss muscular dystrophy, Dunnigan-type familial partial lipodystrophy (FPLD), and cardiomyopathy (*LMNA* mutations are frequent in heart transplant patients; Cowan *et al.*, 2010), and multisystem disorders, including Hutchinson–Gilford progeria syndrome (HGPS; Worman, 2012). Disrupted nucleoskeletal organization and lamin A missense mutations (e.g., G411D, G631D) are also seen relatively frequently in patients with metabolic syndrome, suggesting this too is a laminopathy (Dutour *et al.*, 2011). The molecular mechanisms and tissue specificity of these diseases are poorly understood.

Lamins are extensively posttranslationally modified. The lamin A precursor polypeptide is C-terminally farnesylated and carboxymethylated and then proteolytically cleaved at Y646 to generate mature lamin A (Dechat *et al.*, 2010a). Mature lamin A can be acetylated (Choudhary *et al.*, 2009), *O*-GlcNAcylated (Wang *et al.*, 2010; Alfaro *et al.*, 2012), or Ser/Thr/Tyr-phosphorylated (Eggert *et al.*, 1993; Haas and Jost, 1993; Olsen *et al.*, 2006, 2010; Pan *et al.*, 2009; Wang *et al.*, 2010; Rigbolt *et al.*, 2011) at various positions or SUMOylated by SUMO2 in the rod domain (Zhang and Sarge, 2008) or SUMO3 in the tail domain (Galisson *et al.*, 2011). The tail domain of mature lamin A, comprising residues 385–646, interacts with at least 21 specific partners, including actin (Simon *et al.*, 2010), titin (Zastrow *et al.*, 2006), emerin (Clements *et al.*, 2000), and the transcription factor sterol response element–binding protein 1 (SREBP1; Lloyd *et al.*, 2002). Motivated by predicted SUMOylation site(s) (see later discussion), we explored potential SUMO modification of the lamin A tail.

RESULTS

Because usually only a small percentage, at most, of endogenous SUMO substrates are modified at any given time (Johnson, 2004; Hay, 2005), we adapted a method used routinely in this field, namely transient coexpression assays (Sarge and Park-Sarge, 2009), to independently determine if lamin A is SUMO modified in vivo. Cos-7 cells were transiently cotransfected with full-length mature lamin A (myc tagged at the N-terminus [myc-lamin A]) plus histidine (His)-tagged SUMO1, His-SUMO2, or empty His vector (negative control). Whole-cell protein lysates were prepared 36 h after transfection, incubated with Ni^{2+} beads, and pelleted to affinity purify both free and protein-conjugated His-SUMO. Pelleted proteins were resolved by SDS–PAGE and Western blotted with antibodies specific for myc (Figure 1A). Unmodified myc-lamin A has a natural "His tag" (residues 563–566) that binds Ni^{2+} beads and served as the loading control (Figure 1A, myc-lamA, major ~70-kDa band). An additional minor band at ~125 kDa was detected weakly in cells that expressed myc-lamin A alone and might represent myc-lamin A that was modified by endogenous SUMO1. The ~125-kDa signal was consistently greater in cells that also expressed either His-SUMO1 or His-SUMO2 (Figure 1A). We concluded that this ~125-kDa band was SUMOylated lamin A. These results independently validated the previous report of SUMO2 modification of full-length lamin A (Zhang and Sarge, 2008) and further suggested novel lamin A modification by SUMO1.

In vitro SUMOylation of purified lamin A tails

To specifically investigate lamin A tail SUMOylation, we incubated purified recombinant lamin A tail polypeptides (wild-type mature tail [mA] residues 394–646, wild-type precursor tail [pA] residues 394–664, and the HGPS-causing 50-residue-deleted precursor tail [Δ50]) with recombinant purified SUMO E1 activating enzyme, SUMO E2 conjugating enzyme, and SUMO1, with or without ATP. Reactions were stopped by adding SDS-sample buffer, resolved by SDS–PAGE, and either visualized by Coomassie blue or immunoblotted with antibodies specific for SUMO1 or the T7 tag on lamin tails (Figure 1B). Unmodified lamin A tails migrated at ~34–36 kDa (Figure 1B; single asterisk). All three tails were efficiently modified by SUMO1 (~52–54 kDa; Figure 1B; double asterisks), suggesting that residues 609–659, which are deleted in HGPS, contain no major SUMOylation sites. We also detected a minor slow-migrating (~60- to 70-kDa) T7-tagged lamin A band in all reactions, independent of SUMOylation.

To determine whether lamin A tails were preferentially modified by SUMO1 versus SUMO2, we incubated mature wild-type lamin A

tails with SUMO1, SUMO2, or both for 1 h, then resolved by SDS–PAGE and immunoblotted with antibodies specific for SUMO1 (Figure 1C, lanes 1–3), SUMO2 (Figure 1C, lanes 4–6), or lamin A (Figure 1C, lanes 7–9). In this competition assay, lamin A tail modification by SUMO1 was qualitatively unaffected by the presence of SUMO2 (Figure 1C, α-SUMO1, lane 2 vs. lane 3), suggesting a preference for SUMO1. Supporting this interpretation, modification of the lamin A tail by SUMO2 (Figure 1C, lane 5) was competed by the presence of SUMO1 (Figure 1C, α-SUMO2, lane 6). Thus, under these conditions, the E2 conjugating enzyme preferentially attached SUMO1 to the lamin A tail. Because our in vitro reactions lacked isopeptidases (enzymes that remove SUMO1 or SUMO2/3 and thereby influence preference indirectly in cells; Zhu *et al.*, 2009), we speculate that lamin A tails might associate with SUMO noncovalently, with potentially higher affinity for SUMO1 than SUMO2, thereby increasing the probability that the SUMOylation machinery chooses SUMO1.

In vitro and in vivo analysis of K-to-R–mutated lamin A tail polypeptides

Three different algorithms (SUMOsp2.0, SUMO plot, and PCI-SUMO) were used to predict potential SUMOylation sites in the precursor lamin A tail (Figure 2A). All three predicted SUMOylation at residue K420, with additional sites predicted at K470, K490, K515, or K597 by a single algorithm. K420 is part of the nuclear localization signal (NLS) in lamin A (Dechat *et al.*, 2010a; Dittmer and Misteli, 2011) and is therefore presumably surface exposed. Residues K470, K490, and K515 are exposed on the surface of the lamin A tail Ig-fold domain (Figure 2B, shaded region; Figure 2C shows atomic structure from Krimm *et al.*, 2002), whereas K597 is located outside the Ig-fold in an area of undetermined structure. Further analysis focused on the predicted NLS and Ig-fold sites.

We used site-directed mutagenesis to generate recombinant mature lamin A tails (residues 394–646) with single K-to-R mutations at K420, K470, K490, K515, or, as a predicted negative control, K486 (Figure 2B). The K470R polypeptide was expressed very poorly in bacteria and was not studied further. Each purified lamin A tail polypeptide was incubated in vitro in the presence of SUMO1 and ATP. Reactions were resolved by SDS–PAGE and first immunoblotted with antibodies specific for lamin A and then stripped and reprobed with antibodies to SUMO1 (Figure 2D). The K490R and K515R polypeptides were SUMOylated as efficiently as the wild-type lamin A tail (Figure 2D), suggesting that K490 and K515 were not involved in SUMOylation. However, the K420R and K486R polypeptides had consistently reduced or undetectable SUMOylation compared with wild type (Figure 2D), suggesting that K420 and K486 either were SUMO1 modification sites or required for SUMOylation of the lamin A tail. We were surprised by the K486R result, since this was not a predicted site.

To test the potential biological significance of these Lys residues, we transiently coexpressed myc-tagged, full-length mature lamin A (myc-lamin A; wild type or each K-to-R mutant) with His-SUMO1 or the empty His vector in Cos-7 cells. Whole-cell protein lysates were prepared 36 h after transfection, incubated with Ni^{2+} beads, and pelleted to affinity purify His-SUMO1 and both endogenous and myc-tagged lamin A due to its natural His tag (residues 563–566). Pelleted proteins were resolved by SDS–PAGE and immunoblotted with myc-specific antibodies (Figure 2E). Wild-type myc-lamin A and the K490R and K515R mutants were SUMO1 modified at similar levels in vivo (Figure 2E), consistent with our in vitro results (Figure 2D). Also consistently, the K420R and K486R mutations each substantially reduced lamin A SUMO1 modification in vivo (Figure 2E). Control fluorescence imaging of transfected HeLa cells showed that at low to medium expression levels, green fluorescent protein (GFP)-tagged, full-length mature lamin A polypeptides (wild type or each K-to-R mutant) localized as expected and did not grossly perturb nuclear morphology (Figure 2F). We concluded that the lamin A tail domain is modified both in vitro and in vivo by SUMO1 and that this modification targets at least two residues: consensus residue K420 and totally unexpected residue K486.

FPLD-causing R482Q, K486N, or G465D mutations and lamin A tail SUMOylation

For most laminopathies, disease-causing missense mutations map throughout the lamin A molecule (Dittmer and Misteli, 2011). Of the 24 different residues mutated in FPLD, 16 are located in the tail (Shackleton *et al.*, 2000; Speckman *et al.*, 2000; Haque *et al.*, 2003; Dittmer and Misteli, 2011; Le Dour *et al.*, 2011), and of these 16, 7 (R439, G465, R471, R482, K486, I497, K515E; see later discussion) map to the Ig-fold surface (Dhe-Paganon *et al.*, 2002; Krimm *et al.*, 2002). Our evidence revealed one (K515) as nonessential for SUMO1 modification and another (K486) as critical for SUMO1 modification. This suggested that FLPD disease might arise, at least in part, by disrupted SUMO1 modification of the lamin A tail. We first tested this hypothesis for FPLD-linked mutations G465D, R482Q, and K486N (Figure 3A) in vitro by SUMO1 modification of recombinant lamin A tail residues 385–646 (wild type, G465D, R482Q, or K486N), resolving by SDS–PAGE and sequential immunoblotting for SUMO1 and then lamin A (Figure 3B). The G465D and K486N mutations each reduced lamin A modification by SUMO1 (Figure 3B), whereas R482Q and wild-type tails were modified to similar extents (Figure 3B).

To determine whether these disease-causing mutations also affected lamin A SUMOylation in cells, we cotransfected Cos-7 cells with myc-lamin A (wild type, G465D, R482Q, or K486N) plus either His-SUMO1 or His-SUMO2. Consistent with the biochemical results (Figure 3B), myc-lamin A bearing either G465D or K486N reduced modification by SUMO1 in cells relative to wild-type myc-lamin A (Figure 3C, lanes 4 and 6 vs. lane 3). Also consistently, the R482Q mutation did not reduce SUMO1 modification in cells (Figure 3C, lane 5 vs. lane 3). SUMOylation by SUMO2 in vivo was not grossly affected by these FPLD-causing mutations, with one exception: R482Q appeared to slightly reduce modification by SUMO2 (Figure 3C, lanes 7–10).

SUMOylation-recognition surface motif in the lamin A tail

The foregoing experiments identified K486 as either SUMOylated or required for SUMOylation of the lamin A tail. However, this residue did not match any known SUMOylation consensus motif, all of which have negatively charged (acidic) residues near the modified lysine. To solve this conundrum, we considered whether acidic residues were provided by polypeptide folding. Indeed, four acidic residues are surface exposed near K486 in the Ig-fold structure as shown in Figure 4A: E460 and D461 (directly below K486), and E536 and E537 (close to K486 but on a different side). We hypothesized that one or more of these acidic residues provide the SUMOylation-recognition motif for K486.

To test this model, we analyzed in vitro SUMOylation of T7-tagged lamin A tails (residues 385–646) bearing a single Ala substitution at E460, D461, E536, or E537 or the double mutation E460A/D461A or E536A/E537A. For these experiments, reactions were resolved by SDS–PAGE using 3-(*N*-morpholino)propanesulfonic acid buffer (instead of 2-(*N*-morpholino)ethanesulfonic acid buffer, as in Figure 1B) to improve band resolution, and blots were probed with more sensitive antibodies to the T7 tag on lamin A (not lamin A

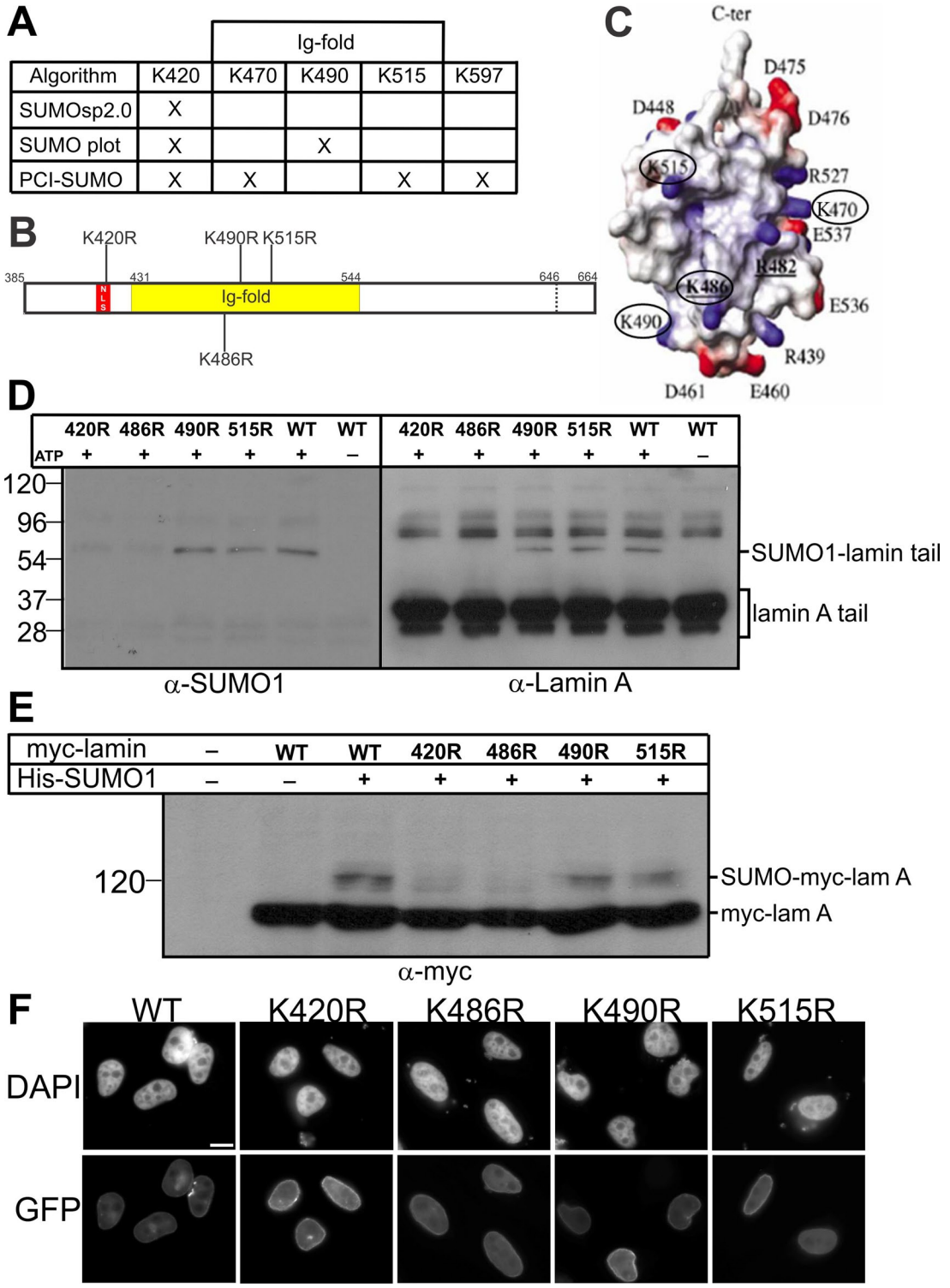

FIGURE 2: Testing predicted SUMOylation sites in the lamin A tail. (A) SUMOylated lysine (K) sites predicted by each algorithm are marked by X. (B) Schematic diagram showing predicted SUMOylation sites and residue K486 in the lamin A tail; the NLS is red, and the Ig-fold (residues 436–552) is yellow. (C) Structure of the lamin A tail Ig-fold from Krimm *et al.* (2002); predicted SUMOylation residues K470, K490, K515, and "control" residue K486 are circled. (D) Mature wild-type or K-to-R–mutated lamin A tails were incubated with SUMO1, E1, and E2 with or without ATP for 1 h at 30°C. Reactions were resolved by SDS–PAGE and immunoblotted sequentially for SUMO1 (α-SUMO1) and then lamin A (α-lamin A); $n = 3$. (E) Mature wild-type or K-to-R–mutated full-length myc-lamin A was transfected into Cos-7 cells alone, or cotransfected with His-SUMO1, for 36 h. Whole-cell lysates were then incubated with Ni^{2+} beads to pellet His-SUMO1 (and lamin A), resolved by SDS–PAGE, and immunoblotted with antibodies to myc (α-myc); $n = 3$. (F) Mature wild-type or K-to-R–mutated full-length GFP-lamin A was transfected into HeLa cells for 24 h. Cells were visualized using DAPI or GFP autofluorescence. Scale bar, 10 μm.

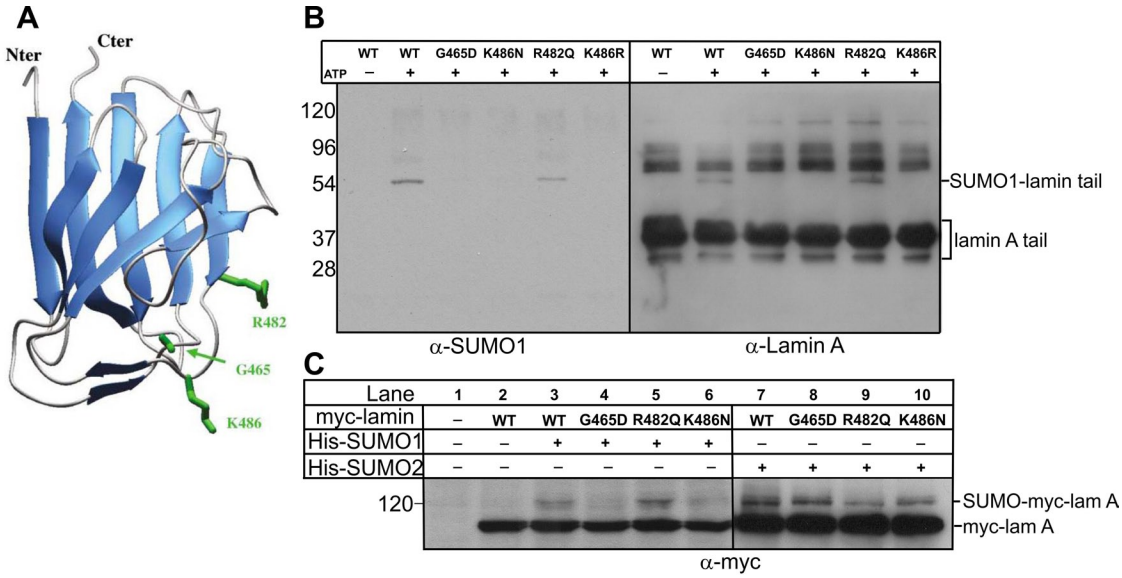

FIGURE 3: Effects of FPLD-causing mutations on lamin A modification by SUMO1 or SUMO2 in vitro and in vivo. (A) Structure of the lamin A tail Ig-fold from Krimm *et al.* (2002) indicating three residues (G465, R482, K486) in which mutations cause FPLD. (B) Mature lamin A tails (wild type or FPLD mutated) were incubated with SUMO1, E1, and E2 with or without ATP for 1 h at 30°C. Reactions were resolved by SDS–PAGE and immunoblotted sequentially for SUMO1 (α-SUMO1) or lamin A (α-lamin A); $n = 3$. (C) Mature myc-lamin A (wild type or FPLD mutated) was cotransfected into Cos-7 cells with His-SUMO1 or His-SUMO2 (or neither) for 36 h. Whole-cell lysates were then incubated with Ni^{2+} beads to pellet His-SUMO1 (and lamin A), resolved by SDS–PAGE, and immunoblotted with antibodies to myc (α-myc); $n = 3$.

antibodies) to ensure equal recognition of mutated lamin tail polypeptides. Results were quantified by densitometry as a percentage of the SUMOylated wild-type T7-lamin A signal (Figure 4C). This analysis revealed at least three ~50.2- to 54.5-kDa (presumably singly modified) lamin-SUMO1 bands; we speculate that SDS–PAGE migration might be slightly different, depending on which site is modified. The E460A, D461A, and double E460A/D461A mutations each reduced lamin A modification by SUMO1 by 65–80%, similar to the effect of G465D or K486N (Figure 4C; $n \geq 3$). This result supported the hypothesis that E460 and D461 provide acidic-residue support for lamin A recognition by the SUMOylation machinery. The other tested mutations (E536A, E537A, E536A/E537A) reduced SUMO1 modification by 30–50% (Figure 4C; $n \geq 3$), suggesting that these acidic residues are less important than E460 and D461 but nevertheless contribute, either to E2 enzyme recognition of lamin A or to the speculative noncovalent association of lamin A with SUMO1.

DISCUSSION

We discovered that the lamin A tail domain is modified, both in vitro and in Cos-7 cells, by SUMO1. This modification, as well as its locations in the lamin molecule (NLS and Ig-fold domain of the lamin A tail) and disease implications, are all distinctly different from the previously reported SUMO2 modification of the lamin A coiled-coil "rod" domain (Zhang and Sarge, 2008). SUMO1 modification of the lamin A tail targets at least two residues: highly predicted residue K420 and totally unexpected residue K486. Of importance, lamin C residues 1–566 are identical to lamin A, suggesting that lamin C might also be modified by SUMO1.

Like other SUMO targets (Gareau and Lima, 2010; Wilkinson and Henley, 2010), SUMO1 modification of lamin A/C is likely to be dynamic. For example, residue 420 can alternatively be modified by SUMO3 (Galisson *et al.*, 2011) or ubiquitin (Kim *et al.*, 2011a) and is surrounded by known phosphorylation sites (Malik *et al.*, 2009; Olsen *et al.*, 2010). Residue 486 has one known alternative modification (ubiquitin; Kim *et al.*, 2011a). SUMOylation at this site might also be dynamically regulated by phosphorylation of nearby surface-exposed Ig-fold residues (Olsen *et al.*, 2010; Kim *et al.*, 2011a; Simon and Wilson, in press).

We propose that SUMO1 modification of K420 within the NLS might inhibit lamin A/C binding to partners such as cyclin D3 or core histones that require an unmodified NLS (Taniura *et al.*, 1995; Zastrow *et al.*, 2004; Mariappan *et al.*, 2007). We further propose that SUMO1 modification of K420 might inhibit lamin A/C binding to α-importin as a potential mechanism for controlling the assembly of A-type lamin filaments after mitosis (Adam *et al.*, 2008). Alternative modification of K420 by SUMO3 in HEK293 cells (Galisson *et al.*, 2011) adds further interest to this site. We found that lamin A tails were modified in vitro by SUMO2 in the absence of SUMO1 but at much lower levels than by SUMO1. Thus, given a choice, the SUMOylation machinery preferentially attached SUMO1 to the lamin A tail in vitro. The mechanism and consequences of this preference for SUMO1 are unknown and will be important to determine in future.

We focused on residue K486, which was critical for SUMO1 modification but located in a region that lacked a canonical linear SUMOylation consensus motif. Our findings support the hypothesis that negatively charged residues required for SUMO-E2 enzyme recognition are provided by the three-dimensional conformation of the Ig-fold domain. SUMOylation machinery recognition and modification of K486 can be explained by a surface consensus "patch" formed by acidic residues E460 and D461 (directly "beneath" K486), each of which was critical for SUMO1 modification. Two other acidic residues, E536 and E537, may provide backup recognition sites since single and double E536A and E537A mutations caused mild defects. To our knowledge this is the first evidence of a "conformational" consensus site for SUMOylation.

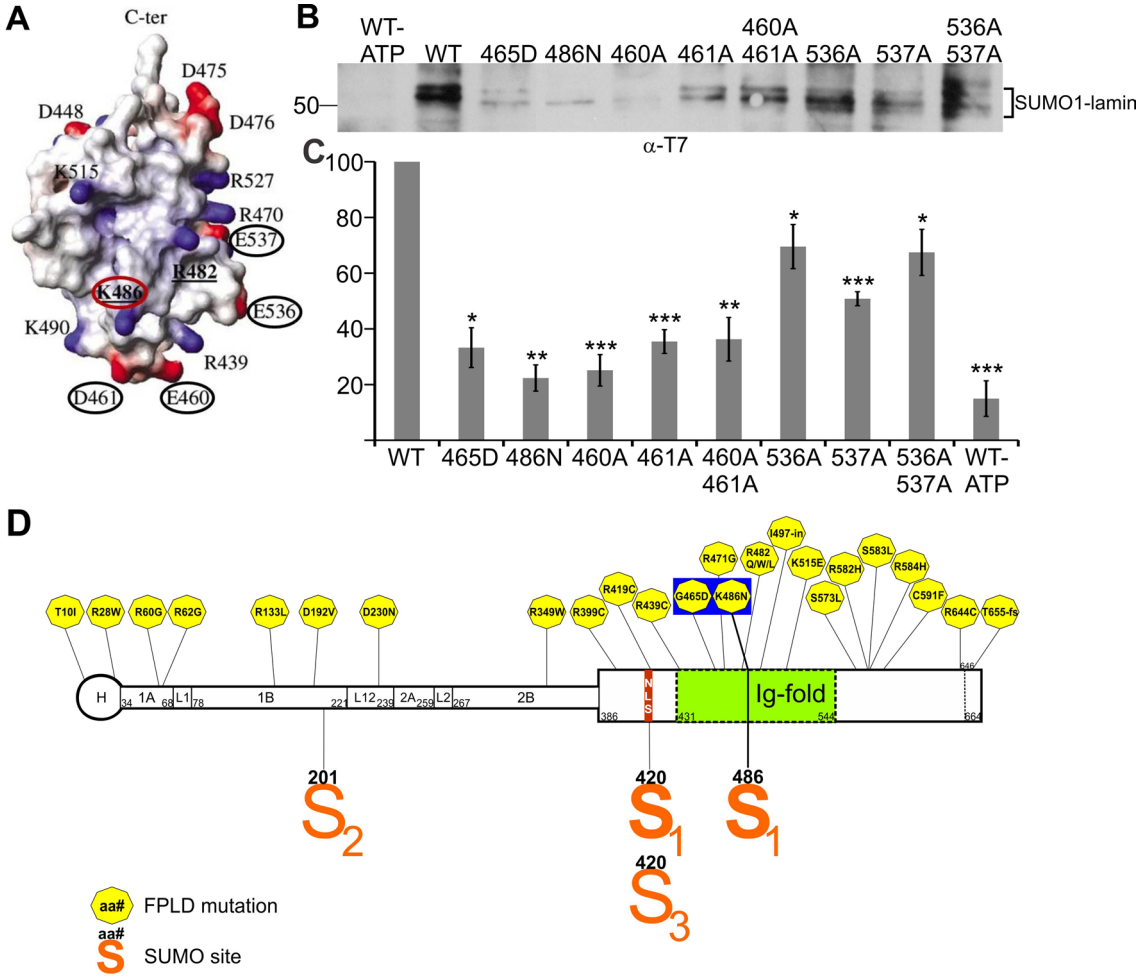

FIGURE 4: Effects of alanine substitutions at acidic residues near K486. (A) Structure of the lamin A tail Ig-fold from Krimm *et al.* (2002) indicating K486 (red circle) and acidic residues E460, D461, E536, and E537 (black circles) tested for potential relevance to lamin A tail recognition by the E2 enzyme. (B) Mature lamin A tails (wild type or K-to-A substituted, 0.3 μg/μl) were incubated with SUMO1, E1, and E2 with or without ATP for 1 h at 30°C. Reactions were resolved by SDS–PAGE and immunoblotted for the T7 tag. (C) Quantification of B by densitometry of SUMOylated lamin bands (bracket) relative to the wild-type lamin A tail ($n \geq 3$; bars indicate SEM). Differences were significant as determined by Student's *t* test relative to wild-type lamin A tail: $*p < 0.05$, $**p < 0.01$, $***p < 0.005$. (D) Schematic diagram of the lamin A molecule showing locations of FPLD-causing mutations (hexagons) and residues modified by SUMO1 (S_1), SUMO2 (S_2), or SUMO3 (S_3). Residues G465 and K486, noted in the text as located on the "bottom front" side of the Ig-fold, are highlighted.

The critical role of K486 in SUMO1 modification of the lamin A tail is particularly interesting since the K486N mutation causes FPLD (Lloyd *et al.*, 2002). We found that K486N and the nearby FPLD-causing mutation G465D both significantly decreased lamin A tail modification by SUMO1 in vitro and in cells. Of importance, neither mutation affected modification of lamin A by SUMO2 in vivo. Another FPLD-causing mutation in the lamin A/C Ig-fold, R482Q, did not significantly affect modification by SUMO1 but showed a slight decrease in SUMO2 modification in vivo. These findings suggested three conclusions: 1) since R482 is not involved in SUMO1 modification of lamin A/C, it might cause disease by a different mechanism (potentially involving SUMO2), 2) K486 is either directly modified by SUMO1 or required for this modification, and 3) G465 is required for lamin A tail recognition by the SUMOylation machinery.

The molecular mechanisms of FPLD are unknown. One study showed that the FPLD-causing G465D, R482W, and K486N mutations each weakly decreased lamin A binding to SREBP1 (residues 1–463; full-length transcription factor) by 25–40% in vitro (Lloyd *et al.*, 2002). This weakened binding suggested, but did not prove, that SREBP1 contacts this region of the Ig-fold. For example, in a separate study, R482W-mutated and wild-type lamin A tails bound similarly well to a smaller SREBP1 fragment (residues 227–487) in vitro (Duband-Goulet *et al.*, 2011). Most previous studies of FPLD patient cells focused on mutations at residue R482 (Broers *et al.*, 2005; Boguslavsky *et al.*, 2006; Bidault *et al.*, 2011). Whether G465D, K486N, or FPLD-causing mutations elsewhere in lamin A/C (Figure 4D) cause disease by similar or distinct mechanisms is an important question for future work. However, our findings suggest that residues located on the "bottom front" of the Ig-fold (G465, K486, E460, D461; Figure 4D) significantly disrupt SUMO1 modification of the lamin tail. On the other hand, our tested mutations located in other regions of the Ig-fold (R482, K490, K515, E536, E537; Figure 4A), did not significantly affect SUMO1 modification of the lamin tail. We therefore propose that in patients with mutations on the "bottom front" of the Ig-fold, FPLD might arise

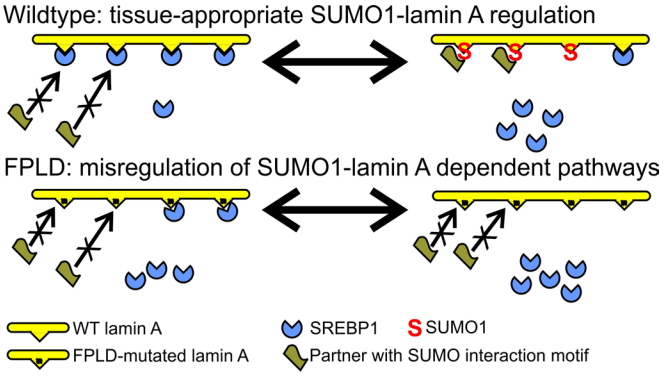

FIGURE 5: Proposed models for SUMO1 regulation of lamin A tails. Proposed mechanisms by which SUMO1 modification of lamin A tails might regulate 1) tissue-appropriate binding or release of SREBP1 (or other partners) and 2) recruitment of hypothetical SIM-containing partner(s) relevant to adipose tissue. We propose that both types of interaction are misregulated in a subset of FPLD patients.

from defective SUMO1 modification, whereas in patients with mutations elsewhere in the Ig-fold or other domains, FPLD arises by a different mechanism.

These findings are significant because they suggest two mechanisms by which SUMO1 might normally contribute to lamin A/C filament regulation in living cells. First, SUMO1 modification at K420 is predicted to block partners that require the unmodified NLS, whereas K486 modification is predicted to block partners (potentially including SREBP1) that require the unmodified Ig-fold (Figure 5). Whether SUMO1 modification of lamin A/C affects the binding or transcriptional activity of SREBP1 is unknown. Second, SUMO1 modification has the potential to recruit or stabilize novel FPLD-relevant partner(s) bearing the SIM motif. In FPLD patients with G465D- or K486N-mutated lamin A/C, we predict both types of partner—SREBP1 and/or other Ig-fold-binding proteins (Zastrow *et al.*, 2004), and hypothetical SIM-containing partner(s)—might be misregulated (Figure 5). These models suggest new ways to think about FPLD disease and explore the differential regulation of lamin A/C function in specific tissues.

MATERIALS AND METHODS

Plasmids and site-directed mutagenesis

Human lamin A tail constructs in pET23b (Novagen, Rockland, MA), which places a His6 tag at the C-terminus and a T7 tag at the N-terminus, for the wild-type mature lamin A tail (residues 394–646) and pre–lamin A tail (residues 394–664) were described previously (Simon *et al.*, 2010). Wild-type FLAG-lamin A mutants R482Q and K486N in pSVK3 were kindly provided by Howard Worman (Columbia University, New York, NY). Wild-type GFP-lamin A in pEGFP-C1 was kindly provided by Kris Dahl (Carnegie Mellon University, Pittsburgh, PA). Single missense mutations in either full-length wild-type lamin A or the lamin A tail were generated by PCR mutagenesis using the primers shown in Supplemental Table S1.

Myc-tagged full-length lamin A or lamin A tail constructs were generated by cloning each wild-type or mutant lamin A into the pCMV-myc vector (Clontech, Mountain View, CA). The SUMO1 and SUMO2 cDNAs were generated by reverse transcription-PCR (RT-PCR) as described (Tatham *et al.*, 2001) using total HeLa cell RNA as template. SUMO cDNAs were cloned into the pcDNA3.1/His vector (Invitrogen, Carlsbad, CA) for expression in mammalian cells. Ubc9 (E2 enzyme) and cDNAs encoding human His-Uba2 and Aos1 (subunits of the E1 enzyme) were kindly provided by Michael Matunis (Johns Hopkins Bloomberg School of Public Health, Baltimore, MD).

Recombinant lamin tails, SUMO1, SUMO2, E1, and E2 enzymes

Recombinant His-tagged lamin tail peptides and His-tagged SUMO1, SUMO2, and human E1 (subunits Uba2 and Aos1) were each expressed separately in *Escherichia coli* BL-21 and purified using nickel-nitriloacetic acid (NTA)–agarose per manufacturer instructions (Qiagen Valencia, CA). Lamin tail peptides were stored in buffer (50 mM $NaHPO_4$, pH 8.0, 300 mM NaCl, 100 mM imidazole, 0.5 mM phenylmethylsulfonyl fluoride) at –80°C. Glutathione *S*-transferase (GST)–tagged E2 was expressed in *E. coli* BL-21 and purified using glutathione–Sepharose 4B (GE Healthcare Bio-Sciences, Piscataway, NJ), and GST was cleaved using factor Xa per manufacturer's instructions (GE Healthcare Bio-Sciences).

In vitro SUMOylation assays and immunoblotting

Each purified recombinant lamin A tail polypeptide was incubated with purified recombinant SUMO1 or SUMO2 plus recombinant-purified E1, E2, and 100 mM ATP as described (Desterro *et al.*, 1998). Reactions were stopped by adding SDS-sample buffer, resolved by SDS–PAGE, transferred to nitrocellulose, and probed using antibodies specific for the lamin A tail (NCL-Lamin A, Novocastra; Leica Microsystems, Buffalo Grove, IL; raised against human lamin residues 598–611; 1:2000 dilution), c-Myc (9E10, Santa Cruz Biotechnology, Santa Cruz, CA; 1:5000), T7 tag (69048-3, Novagen; 1:10,000), SUMO1 (either SC-9060, Santa Cruz Biotechnology, 1:2000; or α-SUMO1, Enzo Life Sciences, Plymouth Meeting, PA; 1:4000), or SUMO2 (α-SUMO2; Enzo Life Sciences; 1:4000). Secondary antibodies were horseradish peroxidase–coupled anti-mouse and anti-rabbit (GE Healthcare, Chalfont St Giles, United Kingdom; 1:10,000).

In vivo SUMOylation assay

Cos-7 cells were transfected with myc-tagged full-length mature lamin A (wild type or each indicated mutant) plus His-SUMO1, His-SUMO2, or the empty His vector as control. Cells were lysed 36 h after transfection, and His-tagged proteins (including lamin A, which has a natural His tag) were affinity enriched under denaturing conditions using nickel NTA-agarose beads (Qiagen) as described previously (Hofmann *et al.*, 2009). After addition of SDS-sample buffer, samples were resolved by SDS–PAGE, transferred to nitrocellulose, probed using antibodies specific for c-Myc (9E10, Santa Cruz Biotechnology; 1:5000), and detected using horseradish peroxidase–coupled anti-mouse secondary antibodies (GE Healthcare; 1:10,000).

HeLa transfections and microscopy

Approximately 60,000 HeLa cells were seeded on glass coverslips (Fisher Scientific, Waltham, MA) and transfected with 3 μg of DNA using LT1 transfection reagent (Roche, Indianapolis, IN). At 24 h after transfection, cells were fixed 15 min in 3% formaldehyde, permeabilized for 20 min in phosphate-buffered saline (PBS)/0.2% Triton X-100, and then blocked for 1 h in PBS/3% bovine serum albumin. DNA was stained using 4′,6-diamidino-2-phenylindole (DAPI), and GFP fluorescence was directly visualized using a Nikon Eclipse E600 equipped with a Nikon Plan APO 60×/numerical aperture 1.40 oil objective (Nikon, Melville, NY). Images were acquired with a Q Imagine Retiga Exi 12-bit digital camera using IP Lab software from Scanalytics (Spectra Services, Ontario, NY).

ACKNOWLEDGMENTS

We gratefully acknowledge Howard Worman and Kris Dahl for lamin constructs, Michael Matunis for E1 and E2 plasmids and insightful discussions, Jason M. Berk for valuable discussions and comments on the manuscript, and research funding from the Department of Defense CDMRP (PC111523 to W.A.H.) and the National Institutes of Health (RO1 048646 to K.L.W.).

REFERENCES

Adam SA, Sengupta K, Goldman RD (2008). Regulation of nuclear lamin polymerization by importin alpha. J Biol Chem 283, 8462–8468.

Alfaro JF *et al.* (2012). Tandem mass spectrometry identifies many mouse brain O-GlcNAcylated proteins including EGF domain-specific O-GlcNAc transferase targets. Proc Natl Acad Sci USA 109, 7280–7285.

Bidault G, Vatier C, Capeau J, Vigouroux C, Bereziat V (2011). LMNA-linked lipodystrophies: from altered fat distribution to cellular alterations. Biochem Soc Trans 39, 1752–1757.

Boguslavsky RL, Stewart CL, Worman HJ (2006). Nuclear lamin A inhibits adipocyte differentiation: implications for Dunnigan-type familial partial lipodystrophy. Hum Mol Genet 15, 653–663.

Broers JL, Kuijpers HJ, Ostlund C, Worman HJ, Endert J, Ramaekers FC (2005). Both lamin A and lamin C mutations cause lamina instability as well as loss of internal nuclear lamin organization. Exp Cell Res 304, 582–592.

Choudhary C, Kumar C, Gnad F, Nielsen ML, Rehman M, Walther TC, Olsen JV, Mann M (2009). Lysine acetylation targets protein complexes and co-regulates major cellular functions. Science 325, 834–840.

Clements L, Manilal S, Love DR, Morris GE (2000). Direct interaction between emerin and lamin A. Biochem Biophys Res Commun 267, 709–714.

Coffinier C, Chang SY, Nobumori C, Tu Y, Farber EA, Toth JI, Fong LG, Young SG (2010). Abnormal development of the cerebral cortex and cerebellum in the setting of lamin B2 deficiency. Proc Natl Acad Sci USA 107, 5076–5081.

Coffinier C *et al.* (2011). Deficiencies in lamin B1 and lamin B2 cause neurodevelopmental defects and distinct nuclear shape abnormalities in neurons. Mol Biol Cell 22, 4683–4693.

Cowan J, Li D, Gonzalez-Quintana J, Morales A, Hershberger RE (2010). Morphological analysis of 13 LMNA variants identified in a cohort of 324 unrelated patients with idiopathic or familial dilated cardiomyopathy. Circ Cardiovasc Genet 3, 6–14.

Dechat T, Adam SA, Taimen P, Shimi T, Goldman RD (2010a). Nuclear lamins. Cold Spring Harb Perspect Biol 2, a000547.

Dechat T, Gesson K, Foisner R (2010b). Lamina-independent lamins in the nuclear interior serve important functions. Cold Spring Harb Symp Quant Biol 75, 533–543.

Dechat T, Pfleghaar K, Sengupta K, Shimi T, Shumaker DK, Solimando L, Goldman RD (2008). Nuclear lamins: major factors in the structural organization and function of the nucleus and chromatin. Genes Dev 22, 832–853.

Desterro JM, Rodriguez MS, Hay RT (1998). SUMO-1 modification of IkappaBalpha inhibits NF-kappaB activation. Mol Cell 2, 233–239.

Dhe-Paganon S, Werner ED, Chi YI, Shoelson SE (2002). Structure of the globular tail of nuclear lamin. J Biol Chem 277, 17381–17384.

Dittmer TA, Misteli T (2011). The lamin protein family. Genome Biol 12, 222.

Duband-Goulet I *et al.* (2011). Subcellular localization of SREBP1 depends on its interaction with the C-terminal region of wild-type and disease related A-type lamins. Exp Cell Res 317, 2800–2813.

Dutour A *et al.* (2011). High prevalence of laminopathies among patients with metabolic syndrome. Hum Mol Genet 20, 3779–3786.

Eggert M, Radomski N, Linder D, Tripier D, Traub P, Jost E (1993). Identification of novel phosphorylation sites in murine A-type lamins. Eur J Biochem 213, 659–671.

Galisson F, Mahrouche L, Courcelles M, Bonneil E, Meloche S, Chelbi-Alix MK, Thibault P (2011). A novel proteomics approach to identify SUMOylated proteins and their modification sites in human cells. Mol Cell Proteomics 10, M110 004796.

Gareau JR, Lima CD (2010). The SUMO pathway: emerging mechanisms that shape specificity, conjugation and recognition. Nat Rev Mol Cell Biol 11, 861–871.

Geiss-Friedlander R, Melchior F (2007). Concepts in sumoylation: a decade on. Nat Rev Mol Cell Biol 8, 947–956.

Gerace L, Huber MD (2012). Nuclear lamina at the crossroads of the cytoplasm and nucleus. J Struct Biol 177, 24–31.

Haas M, Jost E (1993). Functional analysis of phosphorylation sites in human lamin A controlling lamin disassembly, nuclear transport and assembly. Eur J Cell Biol 62, 237–247.

Haque WA, Oral EA, Dietz K, Bowcock AM, Agarwal AK, Garg A (2003). Risk factors for diabetes in familial partial lipodystrophy, Dunnigan variety. Diabetes Care 26, 1350–1355.

Hay RT (2005). SUMO: a history of modification. Mol Cell 18, 1–12.

Hofmann WA, Arduini A, Nicol SM, Camacho CJ, Lessard JL, Fuller-Pace FV, de Lanerolle P (2009). SUMOylation of nuclear actin. J Cell Biol 186, 193–200.

Johnson ES (2004). Protein modification by SUMO. Annu Rev Biochem 73, 355–382.

Kim W *et al.* (2011a). Systematic and quantitative assessment of the ubiquitin-modified proteome. Mol Cell 44, 325–340.

Kim Y, Sharov AA, McDole K, Cheng M, Hao H, Fan CM, Gaiano N, Ko MS, Zheng Y (2011b). Mouse B-type lamins are required for proper organogenesis but not by embryonic stem cells. Science 334, 1706–1710.

Krimm I *et al.* (2002). The Ig-like structure of the C-terminal domain of lamin A/C, mutated in muscular dystrophies, cardiomyopathy, and partial lipodystrophy. Structure 10, 811–823.

Lammerding J, Schulze PC, Takahashi T, Kozlov S, Sullivan T, Kamm RD, Stewart CL, Lee RT (2004). Lamin A/C deficiency causes defective nuclear mechanics and mechanotransduction. J Clin Invest 113, 370–378.

Le Dour *et al.* (2011). A homozygous mutation of prelamin-A preventing its farnesylation and maturation leads to a severe lipodystrophic phenotype: new insights into the pathogenicity of nonfarnesylated prelamin-A. J Clin Endocrinol Metab 96, E856–862.

Lloyd DJ, Trembath RC, Shackleton S (2002). A novel interaction between lamin A and SREBP1: implications for partial lipodystrophy and other laminopathies. Hum Mol Genet 11, 769–777.

Malik R, Lenobel R, Santamaria A, Ries A, Nigg EA, Korner R (2009). Quantitative analysis of the human spindle phosphoproteome at distinct mitotic stages. J Proteome Res 8, 4553–4563.

Mariappan I, Gurung R, Thanumalayan S, Parnaik VK (2007). Identification of cyclin D3 as a new interaction partner of lamin A/C. Biochem Biophys Res Commun 355, 981–985.

Olsen JV, Blagoev B, Gnad F, Macek B, Kumar C, Mortensen P, Mann M (2006). Global, in vivo, and site-specific phosphorylation dynamics in signaling networks. Cell 127, 635–648.

Olsen JV *et al.* (2010). Quantitative phosphoproteomics reveals widespread full phosphorylation site occupancy during mitosis. Sci Signal 3, ra3.

Pan C, Olsen JV, Daub H, Mann M (2009). Global effects of kinase inhibitors on signaling networks revealed by quantitative phosphoproteomics. Mol Cell Proteomics 8, 2796–2808.

Rigbolt KT, Prokhorova TA, Akimov V, Henningsen J, Johansen PT, Kratchmarova I, Kassem M, Mann M, Olsen JV, Blagoev B (2011). System-wide temporal characterization of the proteome and phosphoproteome of human embryonic stem cell differentiation. Sci Signal 4, rs3.

Sarge KD, Park-Sarge OK (2009). Detection of proteins sumoylated in vivo and in vitro. Methods Mol Biol 590, 265–277.

Shackleton *et al.* (2000). LMNA, encoding lamin A/C, is mutated in partial lipodystrophy. Nat Genet 24, 153–156.

Simon DN, Wilson KL (2011). The nucleoskeleton as a genome-associated dynamic "network of networks." Nat Rev Mol Cell Biol 12, 695–708.

Simon DN, Wilson KL (2013). Partners and post-translational modifications of nuclear lamins. Chromosoma (*in press*).

Simon DN, Zastrow MS, Wilson KL (2010). Direct actin binding to A- and B-type lamin tails and actin filament bundling by the lamin A tail. Nucleus 1, 264–272.

Speckman RA, Garg A, Du F, Bennett L, Veile R, Arioglu E, Taylor SI, Lovett M, Bowcock AM (2000). Mutational and haplotype analyses of families with familial partial lipodystrophy (Dunnigan variety) reveal recurrent missense mutations in the globular C-terminal domain of lamin A/C. Am J Hum Genet 66, 1192–1198.

Takamori Y, Tamura Y, Kataoka Y, Cui Y, Seo S, Kanazawa T, Kurokawa K, Yamada H (2007). Differential expression of nuclear lamin, the major component of nuclear lamina, during neurogenesis in two germinal regions of adult rat brain. Eur J Neurosci 25, 1653–1662.

Taniura H, Glass C, Gerace L (1995). A chromatin binding site in the tail domain of nuclear lamins that interacts with core histones. J Cell Biol 131, 33–44.

Tatham MH, Jaffray E, Vaughan OA, Desterro JM, Botting CH, Naismith JH, Hay RT (2001). Polymeric chains of SUMO-2 and SUMO-3 are conjugated to protein substrates by SAE1/SAE2 and Ubc9. J Biol Chem 276, 35368–35374.

Visa N, Percipalle P (2010). Nuclear functions of actin. Cold Spring Harb Perspect Biol 2, a000620.
Wang Z, Udeshi ND, Slawson C, Compton PD, Sakabe K, Cheung WD, Shabanowitz J, Hunt DF, Hart GW (2010). Extensive crosstalk between O-GlcNAcylation and phosphorylation regulates cytokinesis. Sci Signal 3, ra2.
Wilkinson KA, Henley JM (2010). Mechanisms, regulation and consequences of protein SUMOylation. Biochem J 428, 133–145.
Wilson KL, Berk JM (2010). The nuclear envelope at a glance. J Cell Sci 123, 1973–1978.
Wilson KL, Foisner R (2010). Lamin-binding proteins. Cold Spring Harb Perspect Biol 2, a000554.
Worman HJ (2012). Nuclear lamins and laminopathies. J Pathol 226, 316–325.
Zastrow MS, Flaherty DB, Benian GM, Wilson KL (2006). Nuclear titin interacts with A- and B-type lamins in vitro and in vivo. J Cell Sci 119, 239–249.
Zastrow MS, Vlcek S, Wilson KL (2004). Proteins that bind A-type lamins: integrating isolated clues. J Cell Sci 117, 979–987.
Zhang YQ, Sarge KD (2008). Sumoylation regulates lamin A function and is lost in lamin A mutants associated with familial cardiomyopathies. J Cell Biol 182, 35–39.
Zhu S, Goeres J, Sixt KM, Bekes M, Zhang XD, Salvesen GS, Matunis MJ (2009). Protection from isopeptidase-mediated deconjugation regulates paralog-selective sumoylation of RanGAP1. Mol Cell 33, 570–580.

POSTER ABSTRACT 1: Presented at the **9th *Annual Celebration of Academic Excellence*, Buffalo, NY, April 2013.**

THE ROLE OF MYOSIN IC ISOFORM A IN PROSTATE CANCER METASTASIS.

Domaradzki, T. and Hofmann, W.A.

The majority of death from cancer is caused by metastasis, the spreading of cancer cells from primary tumors. This ability of cancer cells to migrate requires secretion of factors that enable cell movement. We discovered a novel myosin (isoA) that is selectively overexpressed in prostate cancer tumor tissues and in cells with high metastatic potential. Because isoA belongs to a group of myosins that transport vesicles, our hypothesis is that isoA facilitates metastasis by increasing secretion of these factors. The objective of this study was to determine the effect of isoA expression on vesicle secretion in the prostate cancer cell line PC-3. To this purpose, we generated various isoA expression constructs. We then analyzed the association of these constructs with vesicles by fluorescence microcopy and determined the effect on secretion by measuring the amount of vesicles secreted in response to construct expression. Our data show that isoA associates with secretory vesicles and overexpression of isoA causes an increase in vesicle secretion; a effect that is ablated by mutations in the membrane binding domain of isoA. These data strongly suggest a critical role for isoA in the development of a metastatic phenotype.

POSTER ABSTRACT 2: Presented at the **9th *Annual Celebration of Academic Excellence*, Buffalo, NY, April 2013.**

IDENTIFICATION AND CHARACTERIZATION OF POSTTRANSLATIONAL MODIFICATIONS OF MYOSIN IC.

Schwab, R.S. and Hofmann, W.A.

Myosin IC (MyoIC) is a member of the myosin superfamily. It localizes to the nucleus where it plays important roles in transcription, intranuclear transport, and nuclear export. However, how the nuclear functions of MyoIC are regulated is not understood. We recently identified a novel, nucleus-specific posttranslational modification of MyoIC and showed that nuclear MyoIC is SUMOylated. SUMOylation of proteins is known to have a great number of consequences for the target protein such as changes in transcriptional activity, cellular translocations, and protein-protein interactions. Thus, SUMOylation could play an important role in the regulation of nuclear MyoIC functions. The goal of this project was to characterize this novel modification. Specifically, to identify the sites in MyoIC to which SUMO proteins are attached to and what SUMO protein is involved in this modification. Using in vivo SUMOylation assays, we showed that MyoIC is modified specifically by SUMO2. In addition, by using site directed mutagenesis in combination with in vivo SUMOylation assays, we identified the specific MyoIC amino acid sequence where SUMO is attached to, and created MyoIC mutant constructs that cannot get SUMOylated anymore. These data are an important first step in understanding the physiological consequences of this novel MyoIC modification.